*Smart system of renewable energy storage based on **IN**tegrated E**V**s and b**A**tteries to empower mobile, **D**istributed and centralised **E**nergy storage in the distribution grid*

Deliverable nº:	**D6.4**
Deliverable name:	**Advanced state of health diagnostics tool**
Version:	**1.0**
Release date:	**11/12/2018**
Dissemination level:	**Public**
Status:	**Submitted**
Author:	**VTT** − **Samppa Jenu, Saara Tuurala, Aino Manninen, Marja Myllysilta, Ivan Deviatkin, Kati Koponen, Ari Hentunen**

Document history:

Version	Date of issue	Content and changes	Edited by
0.1	11/09/2018	First draft version	Samppa Jenu
0.2	05/11/2018	Different authors' contributions combined	Samppa Jenu
0.3	19/11/2018	Content updated	Samppa Jenu
0.4	27/11/2018	Ready for peer-review	Samppa Jenu
1.0	11/12/2018	Peer-reviewed and submitted	Samppa Jenu

Peer reviewed by:

Partner	Reviewer
Schneider Electric	Cristobal Cordobes Berraquero
Albena	Dimitar Stanev

Deliverable beneficiaries:

WP / Task
WP6 / T6.3
WP10
WP5 / T5.3, T5.4
WP3 / T3.7

Table of contents

Abbreviations and Acronyms

Acronym	Description
BEV	Battery Electric Vehicle
BMS	Battery Management System
DOD	Depth Of Discharge
DSO	Distribution System Operator
EOL	End Of Life
EV	Electric Vehicle
FCE	Full Cycle Equivalent
HEV	Hybrid Electric Vehicle
GWP	Global Warming Potential
ICA	Incremental Capacity Analysis
LCA	Life Cycle Assessment
LFP	Lithium Iron Phosphate
LIB	Lithium Ion Battery
LMO	Lithium Manganese Oxide
LNO	Lithium Nickel Oxide
LTO	Lithium Titanate Oxide
NCA	Nickel Cobalt Aluminium
NMC/NCM	Nickel Manganese Cobalt
OCV	Open Circuit Voltage
PHEV	Plug-In Electric Vehicle
PV	Photovoltaics
RT	Room Temperature
RUL	Remaining Useful Life
RFB	Redox Flow Battery
SEI	Solid Electrolyte Interface
SOC	State of Charge
SOH	State of Health
VRFB	Vanadium Redox Flow Battery

Glossary

Aging knee	A stage in battery aging, where degradation rate increases rapidly due to change in the dominant aging mechanism.
C-rate	A measure of the rate at which a battery is discharged relative to the manufacturer's rated capacity in ampere-hours. It is also related to the discharge time. For example, if the battery's rated capacity is 40 Ah, then 1C rate is 40 A and the battery is empty after a 1-hour discharge, 2C rate is 80 A and the battery is empty after a 0.5-hour discharge, and C/4 rate is 10 A and the battery is empty after a 4-hour discharge.
Calendar aging	Battery degradation due to increase in the calendar age of the battery.
Calendar life	The length of time a battery can undergo some defined operation before failing to meet its specified end-of-life criteria.
Capacity	The capacity of a battery expresses the maximum available ampere-hours when a full battery is discharged at a certain C-rate until the cut-off voltage is reached.
Cycle	A sequence of a discharge followed by a charge, or a charge followed by a discharge under specified conditions.
Cycle aging	Battery degradation due to charge-discharge cycling of the battery.
Cycle life	The number of cycles, each to specified discharge and charge termination criteria under a specified charge and discharge regime, that a battery can undergo before failing to meet its specified end-of-life criteria.
Cycle depth	Cycle depth (ΔDOD or ΔSOC) describes the depth of a discharge-charge cycle. Cycle depth is usually expressed in percentage.
Degradation stress factor	Degradation stress factors are all the operation practices or circumstances that accelerate the degradation in battery and thus shorten the lifetime of the cell. Also known as the state of health stress factors.
Depth of discharge	The depth of discharge (DOD) is a measure of how much charge has been discharged from a full battery. It is usually expressed in percentage. Closely related to state of charge (DOD=1-SOC). ΔDOD is used to describe the depth of discharge-charge cycles.
Discharge rate	See *C-rate*.
Duty cycle	The operating parameters of a battery including factors such as charge and discharge rates, depth of discharge, cycle length and rest period length.
End of life	The stage at which a battery is not anymore capable to meet its performance criteria regarding capacity or power. There are two commonly used end-of-life criteria for a

	battery: capacity fade of 20%, resulting in 80% of the original capacity, and power fade of 20%, resulting in 80% of the original power and 25% increase in impedance.
State of charge	The state of charge is a measure of how much charge is left in a battery. It is a ratio of the present charge and the full charge, and it is usually expressed in percents.
State of health	The state of health is a measure of ageing. It can be defined for capacity fade and power fade. Typically a battery is considered to be at its end of life when the state of health has decreased to 80%.
Thermal runaway	Thermal runaway occurs in Li-ion batteries when the rate of internal heat generation caused by the exothermic reactions exceeds the rate at which the heat can be expelled. Eventually, the temperature rises rapidly and the battery catches fire and burns at a very high temperature. The fire may catch nearby cells, and eventually, the whole battery may burn down.

Executive summary

One of the main objectives in the INVADE project is to connect electric vehicles and batteries to the grid in order to provide flexibility to the electricity system. This document is part of the INVADE WP6, which focuses on energy storage technologies.

This deliverable includes results from Task 6.2 *Battery state of health and lifetime* and Task 6.4 *Battery safety and lifecycle management*. This document is a continuation of deliverable D6.3 *Simplified state of health diagnostics tool* and updates and completes its contents.

A state of health diagnostics tool developed in Task 6.2 for batteries in INVADE pilots is presented. Results from the analysis of battery lifetime data from the literature are also presented. These results are utilized in the state of health diagnostics tool and in the battery operation optimization tool developed for the INVADE platform in Task 6.3 *Battery techno-economics and optimal operation*.

Battery end of life criteria for first and second life batteries is discussed. Life cycle assessment for INVADE pilots is carried out partly in WP3 Task 3.7 and partly in WP6 Task 6.4. The life cycle assessment related to batteries in INVADE pilots is reported in this document.

1 Introduction

In INVADE, stationary batteries and electric vehicles are integrated to the grid to provide flexibility to the system. This is demonstrated at five INVADE pilot sites: Bulgaria, Norway, The Netherlands, Spain and Germany. The batteries utilized in the pilot sites are Li-ion batteries except the stationary battery at German pilot, which is a Vanadium redox flow battery. More information about pilot batteries is presented in Chapter 2. A state of health diagnostics tool developed in Task 6.2 for pilot batteries is presented in this deliverable. The diagnostics tool is designed for stationary Li-ion batteries.

Battery state of health (SOH) describes the present condition of the battery compared to fresh battery, and it is usually determined based on available capacity. The battery capacity decreases as the cycle and calendar life of the battery increases. More information about the definition of SOH, the degradation of Li-ion batteries, and the degradation stress factors can be found from D6.3 *Simplified state of health diagnostics tool* [1].

To understand the degradation of Li-ion batteries, experimental cycle life and calendar life test results from the literature are analysed and the main degradation stress factors are identified. In Chapter 3, the main stress factors related to cycle aging and calendar aging are presented and degradation stress factor models are formed for all relevant Li-ion chemistries for which sufficient data is available. The degradation stress factor models are utilized in the battery operation optimization tool developed in Task 6.3 and presented in D6.5 *Advanced battery techno-economics tool* [2]. These degradation stress factor models can also be used to estimate the lifetime of the battery as presented in Chapter 4.

The state of health estimation tool for batteries in INVADE pilots is implemented as a stand-alone tool, which can be run on a regular basis for updating the SOH of the battery into the INVADE platform. The SOH tool is based on a degradation model, which utilizes battery measurement data, battery lifetime data and the degradation stress factor models formed in Chapter 3. The operating principle of the degradation model and the implementation of the SOH tool are presented in Chapter 5. Depending on the constraints of the pilots, the periodic diagnostic test proposed in D6.3 *Simplified state of health diagnostics tool* [1] can be used to tune the parameters of the degradation model and thus increase the accuracy of the SOH estimation.

A concept closely related to the battery state of health is the battery end of life (EOL): the state where the battery no longer meets the requirements of the application. The degradation of the battery weakens the battery characteristics and increases safety risks. The end of life criteria for first and second life batteries is discussed in Chapter 6.

The environmental impact of a product throughout its lifecycle is investigated with a technique called life cycle assessment (LCA). The principle of the LCA method and its application to batteries is introduced in Chapter 7. A LCA model for NMC and LFP batteries is presented. Additionally, literature on the LCA of redox flow batteries is surveyed. The benefits of taking into consideration the battery degradation and SOH in battery LCA are also noted.

2 Battery systems in INVADE pilots

Battery systems in the INVADE pilot sites are different and they are used in various applications. More detailed descriptions of the pilots are given in D10.1 [3]. All five INVADE pilot sites have stationary batteries: either residential batteries or larger stationary battery systems. The stationary batteries used in INVADE pilot sites are listed in Table 1.

Pilot	Application	Total capacity	Battery type
Bulgaria	Centralized battery for hotel and restaurant, connected to PVs.	200 kWh	NMC (Samsung SDI, Tesvolt)
Norway	30 residential batteries connected to PVs, EV chargers and smart heating systems.	30 x 10 kWh (residential)	LMO+NMC (AESC Nissan 2nd life)
The Netherlands	Centralized battery next to an office building. Local balancing: solar panels, windmills, EV charging.	138 kWh	NMC (Samsung SDI, Alfen)
Spain	Backup battery storage system connected to the grid. Secures electricity supply for critical buildings. Can also be used to balance production and consumption in the area.	200 kWh (100 kWh for backup, 100 kWh for balancing)	LFP (ThunderSky-Winston)
Germany	Main value stream: Feed-in of the generation peaks of the PV plants (30 kWp) into the battery system (locally controlled). A second value stream: Peak-shaving of the grid (controlled by the IIP).	120 kWh	Vanadium redox flow (Storion)
	10 existing residential batteries connected to PV systems.	2-10 kWh	Lithium ion

Table 1: Applications and characteristics of the batteries used in the INVADE pilot sites.

INVADE pilots use mostly Li-ion batteries: NMC cells in Bulgaria and in the Netherlands, LFP cells in Spain and second life NMC-LMO cells in Norway. The only exception is the German pilot, which has a larger scale stationary Vanadium redox flow battery in addition to its residential Li-ion batteries. The operating principle and thus the aging processes for the redox flow battery are different to those for Li-ion batteries. Typically the degradation is slower in redox flow batteries compared to Li-ion batteries, which results in longer lifetime. Most of this deliverable focuses on Li-ion batteries, except Chapter 7.4, which focuses on the LCA of redox flow batteries. The SOH estimation tool presented in Chapter 5 is designed for large scale stationary Li-ion batteries.

3   Degradation stress factors

This Chapter is an update to Chapter 4 in deliverable D6.3 *Simplified state of health diagnostics tool* [1]. More comprehensive introduction on degradation stress factors is presented in D6.3.

Degradation stress factors are all the operation practices or circumstances that accelerate the degradation in battery and thus shorten the lifetime of the cell. By identifying the stress factors, the battery operating conditions and practices can be optimized within the application limits so that the degradation of the battery is minimized and longer lifetime achieved.

The degradation processes in lithium-ion batteries can be divided into two groups: degradation during cycling (cycle aging) and degradation during storage (calendar aging). The degradation stress factors can be divided correspondingly: stress factors related to cycle ageing (Chapter 3.1) and stress factors related to calendar ageing (Chapter 3.2).

In this Chapter experimental cycle and calendar life test from the literature are analysed to detect the effect of each stress factor on battery lifetime. The degradation stress factor models formed in this Chapter are exploited in the battery operation optimization tool developed for the INVADE platform in Task 6.3 as explained in deliverable D6.5 *Advanced battery techno-economics tool* [2].

3.1   Cycle ageing

Degradation stress factors related to cycle aging include cycle depth (ΔDOD), average SOC during cycling, cell temperature and the magnitude of charge and discharge current. The batteries in INVADE pilots are only operated with low charge and discharge currents so the current stress factor can be excluded from consideration. The most important cycle ageing stress factors for INVADE pilots are cycle depth and average SOC. Depending on the environmental conditions of the battery, the temperature stress factor should also be taken into account.

3.1.1 Cycle depth

Results from experimental cycle life tests with different cycle depths (ΔDOD) collected from the literature are presented in Figure 1. To be able to compare the results, the data sets are normalized based on the cycle life with 100% ΔDOD. In practice, the cycle life (L^{cyc}) at given ΔDOD is multiplied with ΔDOD to obtain the cycle life in equivalent full cycles (FCE), which is then divided by the cycle life with 100% ΔDOD ($L^{cyc}_{\Delta DOD=100\%}$) to obtain the normalized cycle life:

$$L^{cyc}_{normalized} = \frac{\mathrm{L}^{cyc} \times \Delta DOD}{L^{cyc}_{\Delta DOD=100\%}}$$
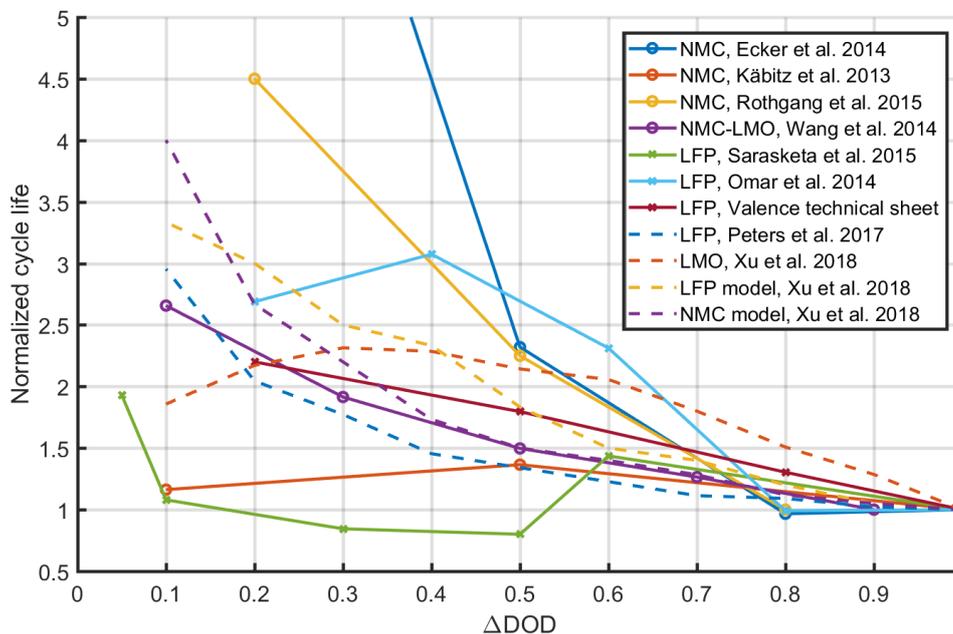

Figure 1: Normalized cycle life of different types of Li-ion cells as a function of ΔDOD. [4] [5] [6] [7] [8] [9] [10] [11] [12]

As Figure 1 shows, the variation between different data sets is large even among the same Li-ion battery chemistry. The overall trend is that the cycle life increases as the ΔDOD decreases, but there is great variation in the magnitude of the increase. Generally, the relation seems to follow exponential curve.

An exponential model is fit to NMC cell data set from Ecker et al. 2014 [4] in Figure 2 and to NMC-LMO cell data set from Wang et al. 2014 [7] in Figure 3. Both cycle depth stress factor models are presented in Table 2. In both cases the exponential model fits well to the data but the magnitude of the lifetime increase is different. The model based on the data from Wang et al. represents fairly average curve from the data sets in Figure 1, whereas the model based on the data from Ecker et al. represents the steeper end.
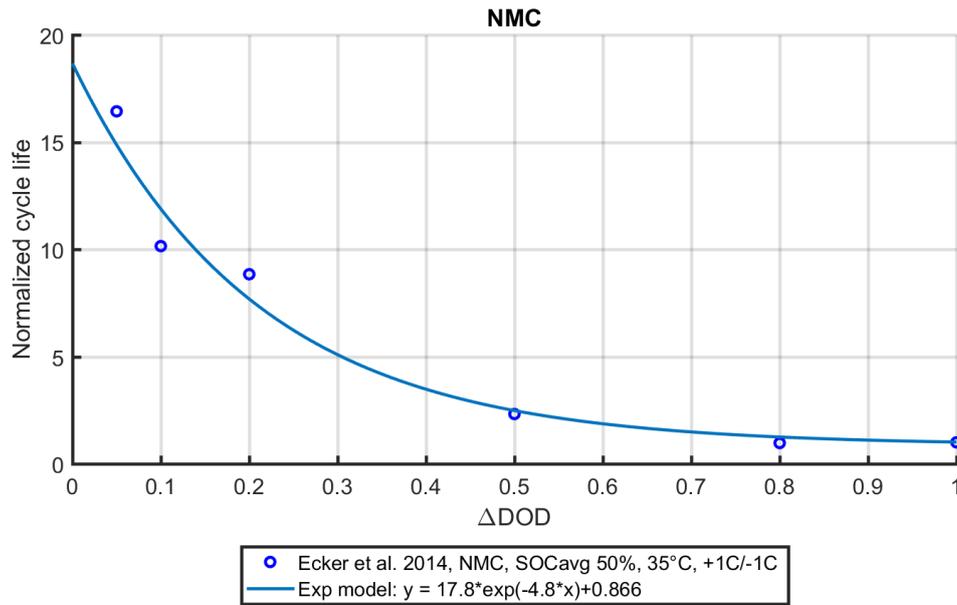
Figure 2: An exponential cycle depth stress factor model fit to experimental NMC cell data from Ecker et al. [4].
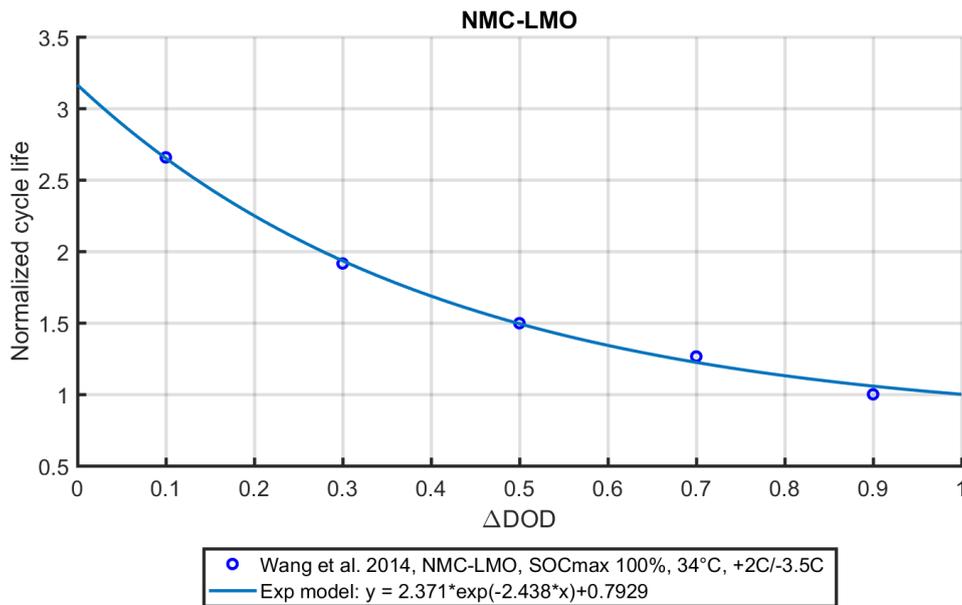

Figure 3: An exponential cycle depth stress factor model fit to experimental NMC-LMO cell data from Wang et al. [7].

Chemistry	Degradation stress factor model	Reference
NMC	$f^{cyc}_{\Delta DOD}(\Delta DOD) = 17.8e^{-4.8\Delta DOD} + 0.866$	Ecker et al. [4]
NMC-LMO	$f^{cyc}_{\Delta DOD}(\Delta DOD) = 2.371e^{-2.438\Delta DOD} + 0.7929$	Wang et al. [7]

Table 2: Cycle depth stress factor models.

3.1.2 Average SOC

Results from experimental cycle life tests with different average SOC values for NMC cell from Ecker et al. 2014 [4] and for LFP cell from Jiang et al. 2014 [13] are presented in Figure 4. The data sets are normalized based on the highest cycle life in the data set. According to these results the longest cycle life is achieved with average SOC close to 50% and the cycle life decreases with low and high average SOC values.
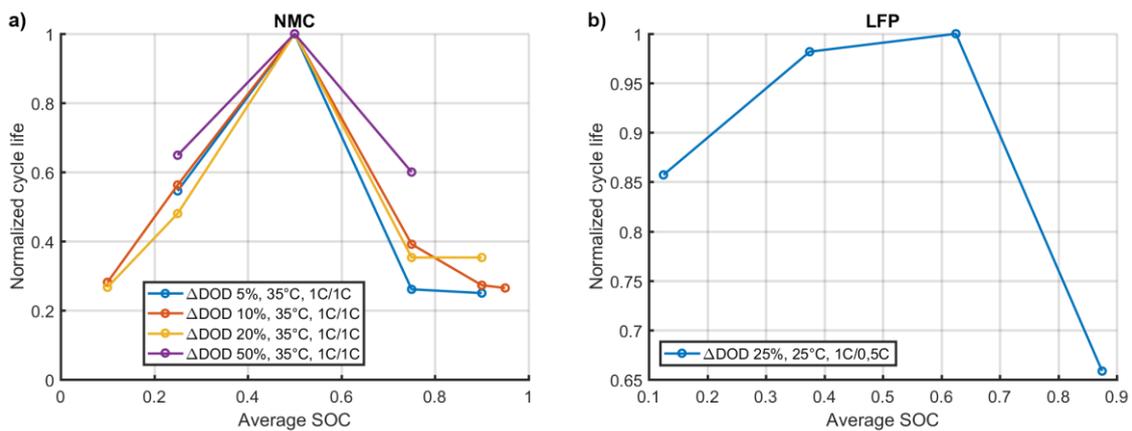

Figure 4: Normalized cycle life of a) NMC cell [4] b) LFP cell [13] as a function of average SOC.

Due to lack of comprehensive data sets, it is difficult to tell the exact shape of the relation between the average SOC and cycle life. In Figure 5, a piecewise Gaussian model is fit to the data from Ecker et al. The Gaussian model seems to be a fairly good approximation based on the data that is available. The stress factor model is presented also in Table 3.
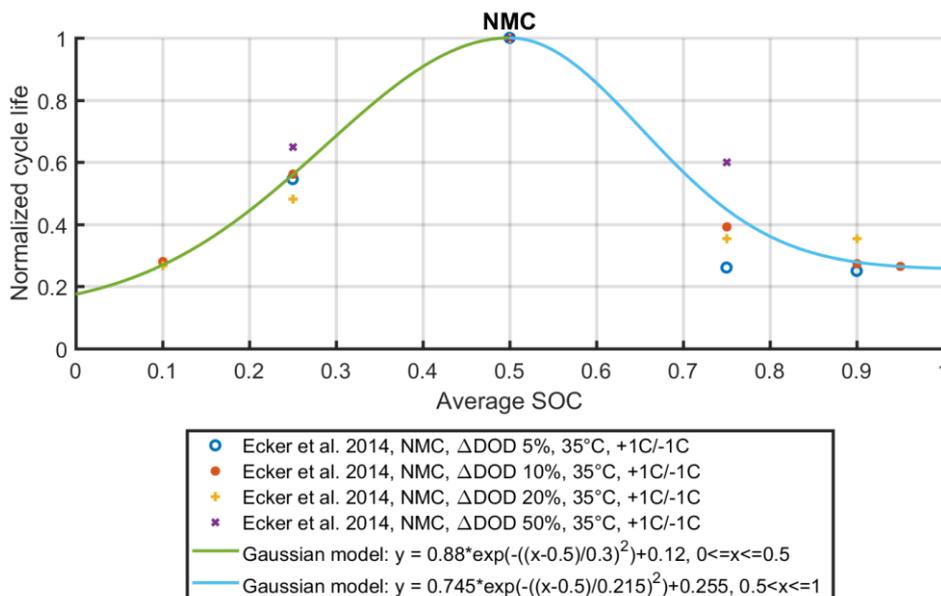

Figure 5: A piecewise Gaussian average SOC stress factor model fit to experimental NMC cell data from Ecker et al. [4].

Chemistry	Degradation stress factor model	Reference
NMC	$f_{SOC}^{cyc}(SOC) = \begin{cases} 0.88e^{-\left(\frac{SOC-0.5}{0.3}\right)^2 + 0.12}, & 0 \leq SOC \leq 0.5 \\ 0.745e^{-\left(\frac{SOC-0.5}{0.215}\right)^2 + 0.255}, & 0.5 < SOC \leq 1 \end{cases}$	Ecker et al. [4]

Table 3: Average SOC stress factor model.

3.1.3 Temperature

Results from experimental cycle life tests with different operating temperatures collected from the literature are presented in Figure 6. The data sets are normalized with respect to the cycle life in room temperature (22-26 °C):

$$L_{normalized}^{cyc} = \frac{L^{cyc}}{L_{RT}^{cyc}}$$
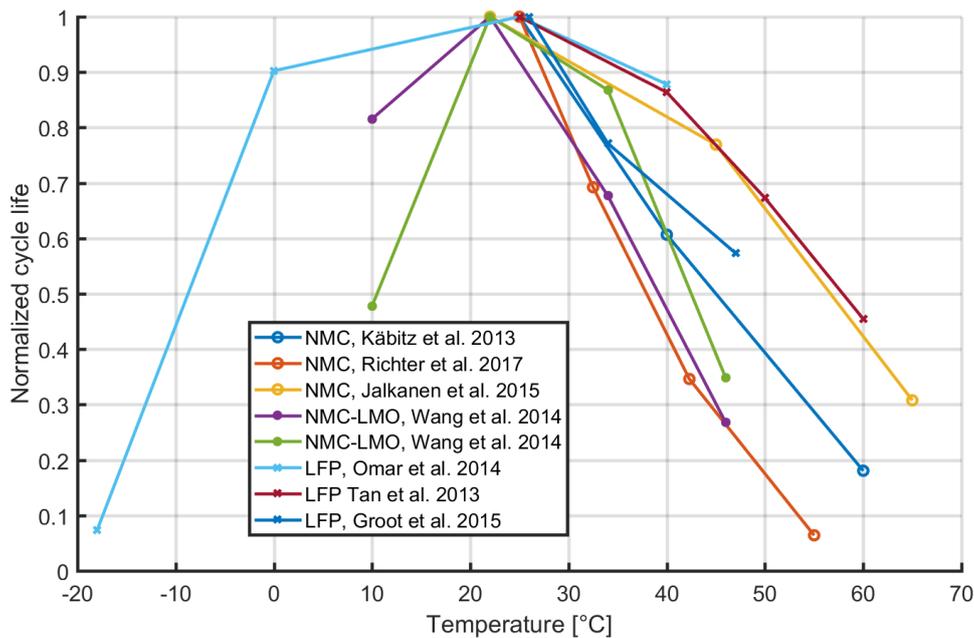
Figure 6: Normalized cycle life of different types of Li-ion cells as a function of temperature. Normalization is done with respect to the cycle life in room temperature (22-26°C). [5] [14] [15] [7] [9] [16] [17]

Figure 6 clearly shows that the cycle life of Li-ion batteries decreases as the operating temperature is increased from the room temperature level. Similarly, the cycle life decreases as the operating temperature is decreased from the room temperature level. However, there are only few data points available from low temperatures, which increases the uncertainties.

A Gaussian model is fit to NMC cell data in Figure 7 and to LFP cell data in Figure 8. In both cases the Gaussian model fits well to the data above room temperature, but in cold temperatures the fitting is challenging due to lack of data points. For both chemistries the optimal operating temperature is around room temperature, but for NMC the cycle life seems to decrease faster when the operating temperature is increased or decreased compared to LFP. Both temperature stress factor models are presented also in Table 4.
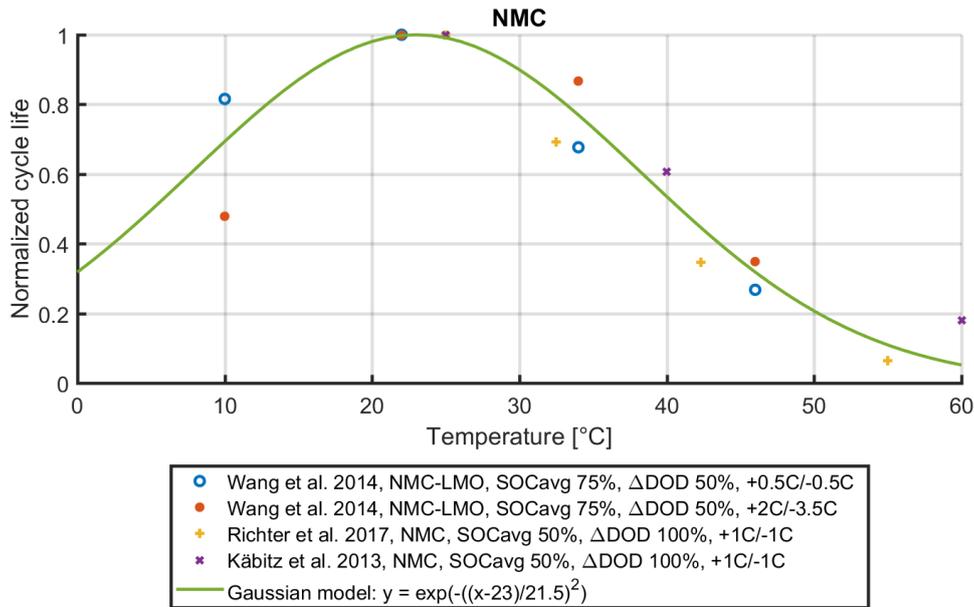
Figure 7: A Gaussian temperature stress factor model fit to experimental NMC-LMO cell data from Wang et al. [7] and NMC cell data from Richter et al. [14] and Käbitz et al. [5].
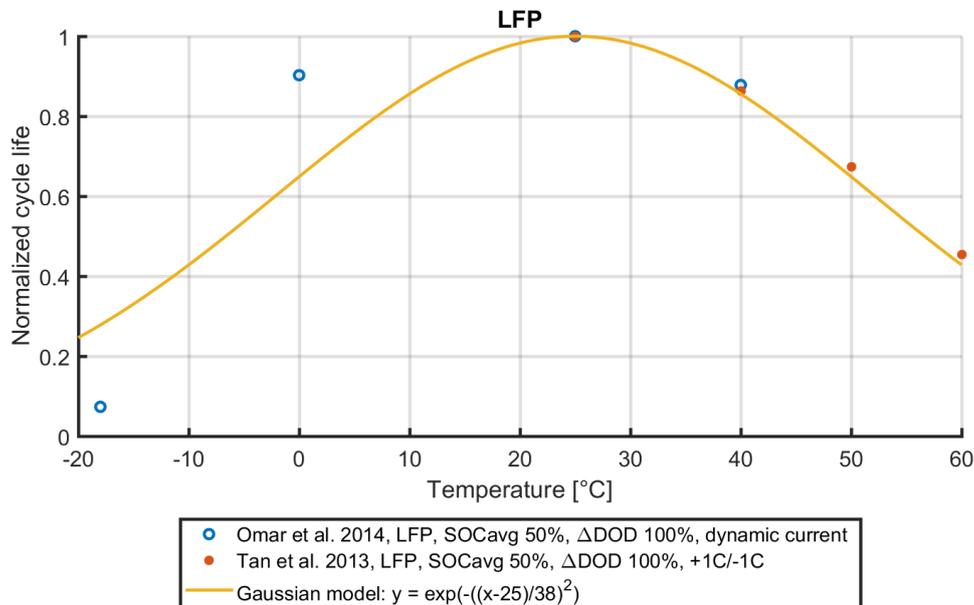
Figure 8: A Gaussian temperature stress factor model fit to experimental LFP cell data from Omar et al. [9] and Tan et al. [16].

Chemistry	Degradation stress factor model	Reference
NMC	$f_T^{cyc}(T) = e^{-\left(\frac{T-23}{21.5}\right)^2}$	Wang et al. [7] Richter et al. [14] Käbitz et al. [5]
LFP	$f_T^{cyc}(T) = e^{-\left(\frac{T-25}{38}\right)^2}$	Omar et al. [9] Tan et al. [16]

Table 4: Cycle aging temperature stress factor models.

3.2   Calendar ageing

The key degradation stress factors related to calendar aging are storage temperature and battery SOC during storage. Battery SOC during idle time is the major calendar aging stress factor, which can be affected by battery usage. The effect of storage temperature on battery calendar life should also be taken into account if the battery is not located in a temperature-controller space or the environmental temperature differs from normal room temperature.

3.2.1   Storage temperature

Results from experimental calendar life tests in different temperatures for NMC chemistry collected from the literature are presented in Figure 9. As can be seen from Figure 9, the calendar life of NMC cells decreases almost linearly as the temperature increases. Consequently, a linear model is fit to NMC cell data in Figure 10. The temperature stress factor model is presented also in Table 5.
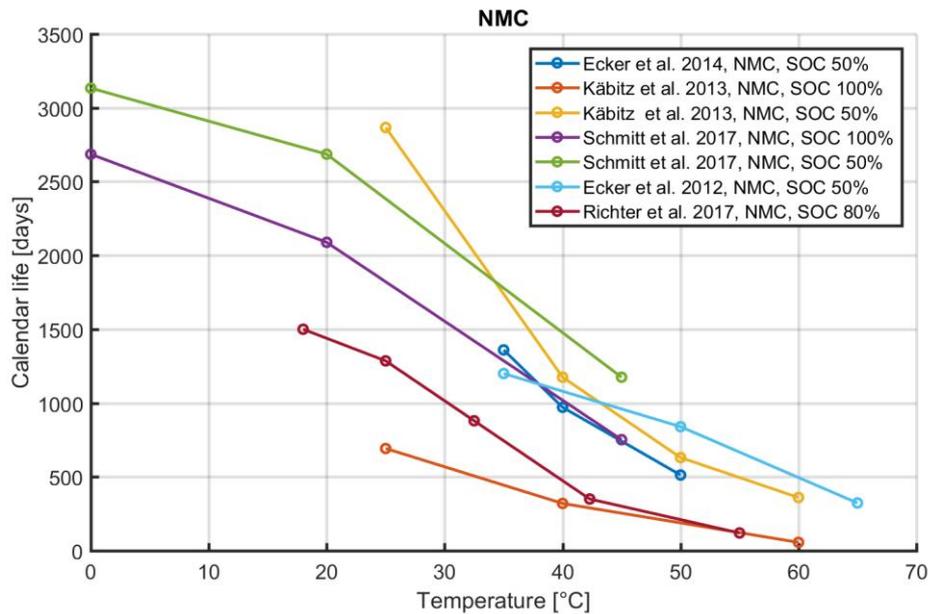
Figure 9: Calendar life of NMC cells as a function of temperature. EOL at 80% SOH (capacity). [4] [5] [18] [19] [14]

Chemistry	Degradation stress factor model	Reference
NMC	$f_T^{cal}(T) = -0.0264T + 1.6067$	Schmitt et al. [18], Richter et al. [14]

Table 5: Calendar aging temperature stress factor model.
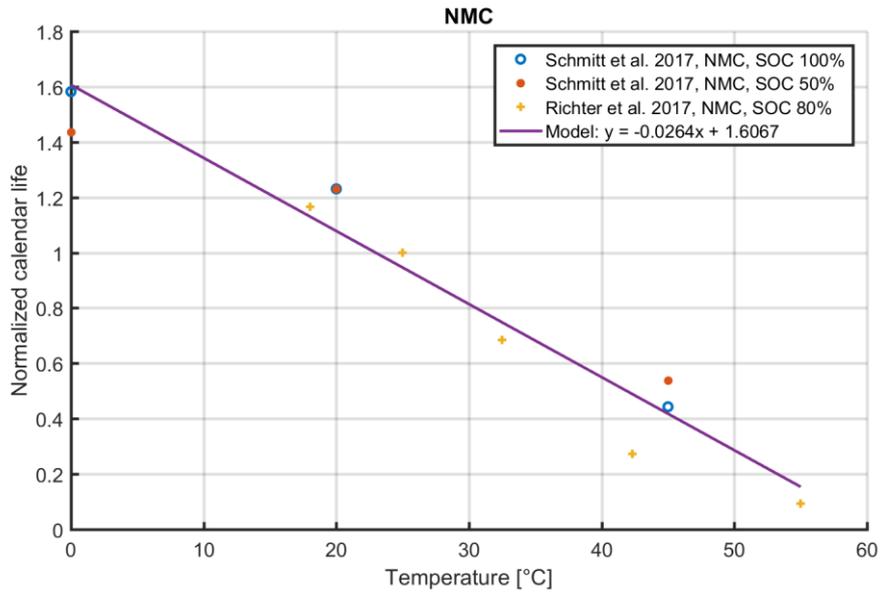
Figure 10: A linear temperature stress factor model for calendar aging of NMC cells. Model is fit to experimental data from Schmitt et al. [18] and Richter et al. [14].

Results from experimental calendar life tests in different temperatures for LFP chemistry collected from the literature are presented in Figure 11. In high temperatures the effect of temperature on calendar life of LFP cells seems to be similar to that of NMC cells. Instead in lower temperatures much longer calendar life is reached with LFP cells according to Lewerenz et al. 2017 [20]. However, the lack of comprehensive data at temperatures below 30 °C makes forming an applicable temperature stress factor model for LFP chemistry unfeasible.
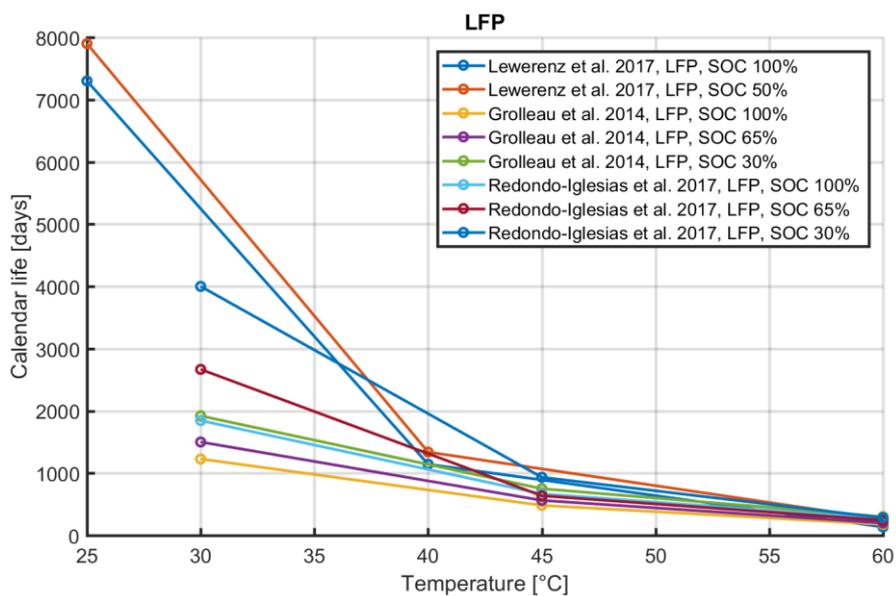
Figure 11: Calendar life of LFP cells as a function of temperature. EOL at 80% SOH (capacity). [20] [21] [22]

3.2.2   Storage SOC

Results from experimental calendar life tests with different storage SOCs collected from the literature are presented in Figure 12. The data sets are normalized with respect to the calendar life with 100% SOC. Variation between the data sets is large, but a clear pattern can be seen: NMC chemistry has the steepest curve, NMC-LMO moderate and LFP the lowest. In Figure 13, an exponential model is fit to data sets from each examined Li-ion chemistry. For each chemistry the exponential model describes the overall trend, but more data sets would be needed for determining more accurate models. For LFP chemistry the change in calendar life as a function of storage SOC is fairly small and it could also be described with a linear model. The storage SOC stress factor models are presented also in Table 6.
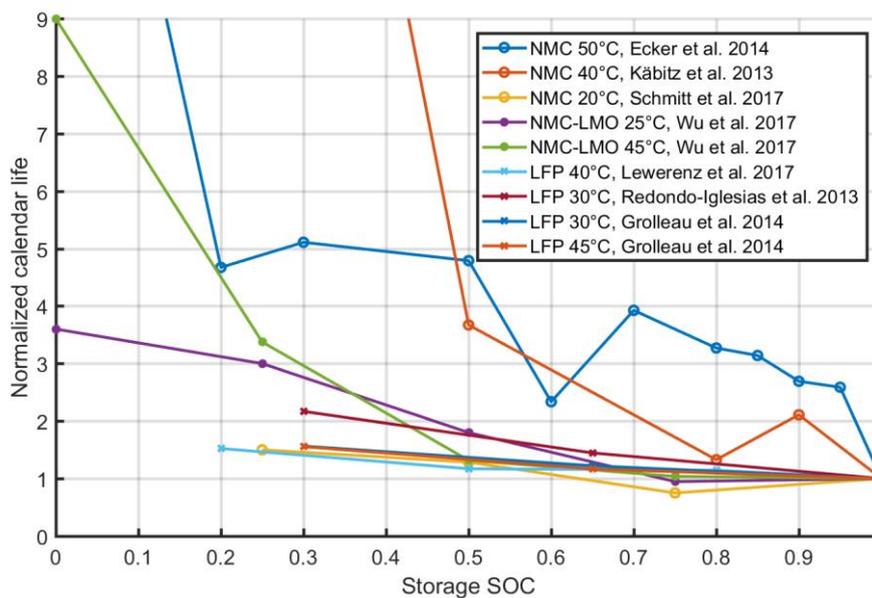
Figure 12: Normalized calendar life of different types of Li-ion cells as a function of storage SOC. [4] [5] [18] [23] [20] [22] [21]
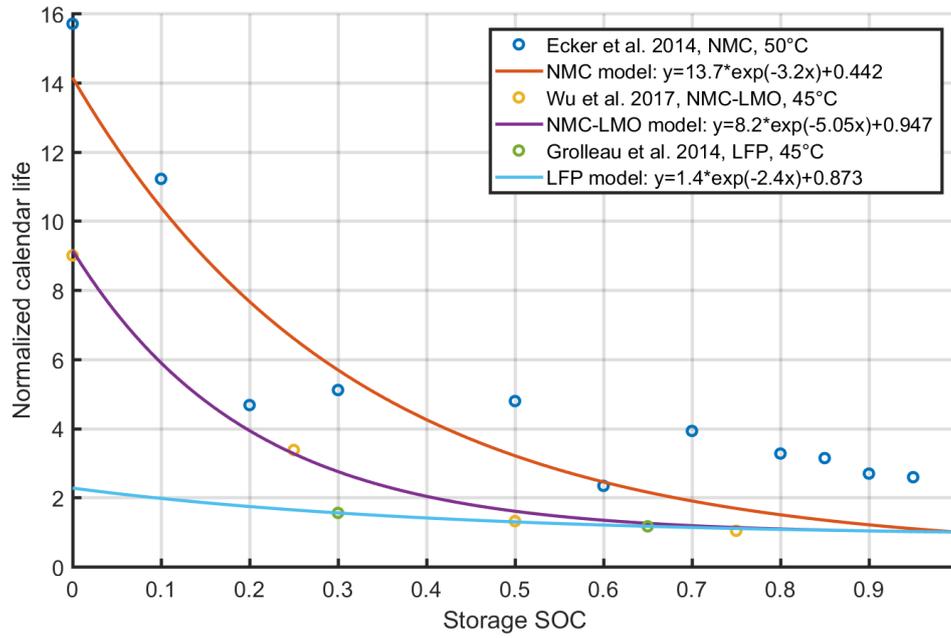
Figure 13: Exponential storage SOC stress factor models fit to experimental NMC cell data from Ecker et al. [4], NMC-LMO cell data from Wu et al. [23] and LFP cell data from Grolleau et al. [21].

Chemistry	Degradation stress factor model	Reference
NMC	$f_{SOC}^{cal}(SOC) = 13.7e^{-3.2SOC} + 0.442$	Ecker et al. [4]
NMC-LMO	$f_{SOC}^{cal}(SOC) = 8.2e^{-5.05SOC} + 0.947$	Wu et al. [23]
LFP	$f_{SOC}^{cal}(SOC) = 1.4e^{-2.4SOC} + 0.873$	Grolleau et al. [21]

Table 6: Storage SOC stress factor models.

4 Li-ion battery lifetime model

Degradation stress factor models formed in Chapter 2 can be combined to produce a lifetime model for estimating the cycle life or calendar life of Li-ion cells in different operating and environmental conditions. As input for the lifetime model a reference lifetime under known conditions is needed. As an example in this Chapter, the lifetime model is formed for Samsung SDI NMC cell, similar to those used in INVADE pilot sites in Bulgaria and the Netherlands.

4.1 Cycle life model

The battery cycle life model estimates the cycle life of the battery considering the main degradation stress factors related to cycle aging, which are cycle depth (ΔDOD), average SOC during cycling and cell temperature. The model estimates battery cycle life L^{cyc} utilizing battery degradation stress factor models:

$$L^{cyc} = \frac{L_{ref}^{cyc}}{S_{\Delta DOD}^{cyc}(\Delta DOD, \Delta DOD_{ref})S_{SOC}^{cyc}(SOC, SOC_{ref})S_T^{cyc}(T, T_{ref})}$$

where L_{ref}^{cyc} is a reference cycle life with reference cycle depth (ΔDOD_{ref}), average SOC (SOC_{ref}) and temperature (T_{ref}). Coefficients $S_{\Delta DOD}^{cyc}$, S_{SOC}^{cyc} and S_T^{cyc} describe the effects of each degradation stress factor on battery cycle life. These stress factor coefficients are based on the degradation stress factor models formed in Chapter 3.1.

The use of the cycle life model is demonstrated for NMC chemistry. The stress factor models utilized for cycle life estimation are presented in Table 7.

Stress factor coefficient	Stress factor model	Model based on data from
$S_{\Delta DOD}^{cyc} = \dfrac{f_{\Delta DOD}^{cyc}(\Delta DOD_{ref})}{f_{\Delta DOD}^{cyc}(\Delta DOD)}$	$f_{\Delta DOD}^{cyc}(\Delta DOD) = 2.371e^{-2.438\Delta DOD} + 0.7929$	Wang et al. [7]
$S_{SOC}^{cyc} = \dfrac{f_{SOC}^{cyc}(SOC_{ref})}{f_{SOC}^{cyc}(SOC)}$	$f_{SOC}^{cyc}(SOC)$ $= \begin{cases} 0.88e^{-\left(\frac{SOC-0.5}{0.3}\right)^2 +0.12}, & 0 \leq SOC \leq 0.5 \\ 0.745e^{-\left(\frac{SOC-0.5}{0.215}\right)^2 +0.255}, & 0.5 < SOC \leq 1 \end{cases}$	Ecker et al. [4]
$S_T^{cyc} = \dfrac{f_T^{cyc}(T_{ref})}{f_T^{cyc}(T)}$	$f_T^{cyc}(T) = e^{-\left(\frac{T-23}{21.5}\right)^2}$	Wang et al. [7] Richter et al. [14] Käbitz et al. [5]

Table 7: Degradation stress factor models used in the cycle life model.

The cycle depth stress factor model based on data from Wang et al. (Figure 3) is used instead of the model based on data from Ecker et al. (Figure 2) as the data from Wang et al. is close to average curve whereas the data from Ecker et al. differs significantly from the average (Figure 1).

The reference cycle life used is 6000 FCE ($\Delta DOD=100\%$, $SOC_{avg}=50\%$, $T=25°C$), which is based on the cycle life promised for Samsung SDI NMC cells [24] [25] [26]. The results of the cycle life model for NMC cell are presented in Figure 14.

a) Estimated cycle life, $\Delta DOD=0.7$ (ref: 6000 FCE, $\Delta DOD=1$, $SOC_{avg}=0.5$, $T=25°C$)

T [°C]	0.1	0.2	0.3	0.4	0.5	0.6	0.7	0.8	0.9
0				2139	2357	2016			
5				3333	3673	3141			
10				4661	5136	4392			
15				5849	6446	5512			
20				6589	7260	6208			
25				6660	7339	6276			
30				6042	6659	5694			
35				4920	5422	4636			
40				3595	3962	3388			
45				2358	2598	2222			
50				1388	1529	1308			
55				733.1	807.9	690.8			

Average SOC

b) Estimated cycle life, $\Delta DOD=0.7$ (ref: 6000 FCE, $\Delta DOD=1$, $SOC_{avg}=0.5$, $T=25°C$)

c) Estimated cycle life, $\Delta DOD=0.5$ (ref: 6000 FCE, $\Delta DOD=1$, $SOC_{avg}=0.5$, $T=25°C$)

T [°C]	0.1	0.2	0.3	0.4	0.5	0.6	0.7	0.8	0.9
0			1969	2612	2878	2461	1637		
5			3069	4070	4485	3835	2550		
10			4291	5691	6272	5363	3566		
15			5386	7143	7871	6730	4475		
20			6066	8045	8865	7581	5041		
25			6132	8132	8962	7663	5095		
30			5563	7378	8130	6952	4623		
35			4530	6007	6620	5661	3764		
40			3310	4390	4838	4137	2751		
45			2171	2879	3173	2713	1804		
50			1278	1695	1867	1597	1062		
55			675	895.2	986.5	843.5	560.9		

Average SOC

d) Estimated cycle life, $\Delta DOD=0.5$ (ref: 6000 FCE, $\Delta DOD=1$, $SOC_{avg}=0.5$, $T=25°C$)

e) Estimated cycle life, $\Delta DOD=0.3$ (ref: 6000 FCE, $\Delta DOD=1$, $SOC_{avg}=0.5$, $T=25°C$)

T [°C]	0.1	0.2	0.3	0.4	0.5	0.6	0.7	0.8	0.9
0		1654	2550	3382	3727	3187	2119	1347	
5		2577	3973	5270	5807	4965	3302	2098	
10		3603	5556	7369	8120	6944	4617	2934	
15		4522	6973	9248	10191	8714	5795	3682	
20		5094	7854	10417	11479	9815	6527	4147	
25		5149	7940	10530	11604	9922	6598	4193	
30		4671	7203	9553	10527	9002	5986	3804	
35		3804	5865	7778	8572	7329	4874	3097	
40		2779	4286	5684	6264	5356	3561	2263	
45		1823	2811	3728	4108	3513	2336	1484	
50		1073	1654	2194	2418	2068	1375	874	
55		567	874	1159	1277	1092	726	461	

Average SOC

**f)** Estimated cycle life, $\Delta DOD=0.3$ (ref: 6000 FCE, $\Delta DOD=1$, $SOC_{avg}=0.5$, $T=25°C$)

Figure 14: Cycle life model results for NMC cell with $\Delta DOD=70\%$ (a, b), $\Delta DOD=50\%$ (c, d) and $\Delta DOD=30\%$ (e, f). The reference value used is 6000 FCE with $\Delta DOD=100\%$, $SOC_{avg}=50\%$, $T=25°C$.

4.2   Calendar life model

The battery calendar life model estimates the calendar life of the battery considering the main degradation stress factors related to calendar aging, which are SOC and temperature during storage. The model estimates battery cycle life L^{cal} utilizing battery degradation stress factor models:

$$L^{cal} = \frac{L^{cal}_{ref}}{S^{cal}_{SOC}(SOC, SOC_{ref})S^{cal}_{T}(T, T_{ref})}$$

where L^{cal}_{ref} is a reference calendar life with reference SOC (*SOC_ref*) and temperature (*T_ref*). Coefficients S^{cal}_{SOC} and S^{cal}_{T} describe the effects of main degradation stress factors on battery calendar life. These stress factor coefficients are based on the degradation stress factor models formed in Chapter 3.2.

The use of the calendar life model is demonstrated for NMC chemistry. The stress factor models utilized for calendar life estimation are presented in Table 8.

Stress factor coefficient	Stress factor model	Model based on data from
$S^{cal}_{SOC} = \dfrac{f^{cal}_{SOC}(SOC_{ref})}{f^{cal}_{SOC}(SOC)}$	$f^{cal}_{SOC}(SOC) = 13.7e^{-3.2SOC} + 0.442$	Ecker et al. [4]
$S^{cal}_{T} = \dfrac{f^{cal}_{T}(T_{ref})}{f^{cal}_{T}(T)}$	$f^{cal}_{T}(T) = -0.0264T + 1.6067$	Schmitt et al. [18] Richter et al. [14]

Table 8: Degradation stress factor models used in the calendar life model.

The reference calendar life used for the model is 10 years (SOC=50% and T=25°C), which is based on the performance warranty of 10 years promised for Samsung SDI NMC cells [26]. The results of the calendar life model for NMC cell are presented in Figure 15.

a)

Estimated calendar life (ref: 10 years, SOC=0.5, T=25°C)

T [°C]	0.1	0.2	0.3	0.4	0.5	0.6	0.7	0.8	0.9
0	54.97	40.56	30.09	22.49	16.97	12.96	10.05	7.941	6.407
5	50.45	37.22	27.62	20.64	15.58	11.9	9.228	7.289	5.881
10	45.94	33.89	25.15	18.79	14.18	10.83	8.402	6.636	5.354
15	41.42	30.56	22.67	16.95	12.79	9.769	7.576	5.984	4.828
20	36.9	27.23	20.2	15.1	11.39	8.704	6.75	5.332	4.301
25	32.39	23.9	17.73	13.25	10	7.639	5.924	4.679	3.775
30	27.87	20.56	15.26	11.4	8.606	6.574	5.098	4.027	3.249
35	23.36	17.23	12.79	9.556	7.211	5.509	4.272	3.374	2.722
40	18.84	13.9	10.31	7.709	5.817	4.444	3.446	2.722	2.196
45	14.32	10.57	7.841	5.861	4.423	3.378	2.62	2.069	1.67
50	9.809	7.237	5.369	4.013	3.028	2.313	1.794	1.417	1.143
55	5.293	3.905	2.897	2.165	1.634	1.248	0.9681	0.7646	0.6169

SOC

b)

Figure 15: Calendar life model results for NMC cell. Reference value used is 10 years with SOC=50% and T=25°C.

5   SOH estimation tool

The SOH estimation tool designed for INVADE pilots is based on an empirical battery degradation model, which combines the effect of degradation stress factors (Chapter 3) with battery lifetime data provided by the battery manufacturer. Taking the stress factors into account increases the accuracy of the degradation model in varying battery environment and operating conditions.

5.1   Degradation model

The degradation model estimates the capacity degradation of the battery occurring during the observation period. The degradation model consists of two parts: cycle degradation model and calendar degradation model. The estimated total degradation is the sum of the outputs of these two submodels. The operating principle of the degradation model is presented in Figure 16.
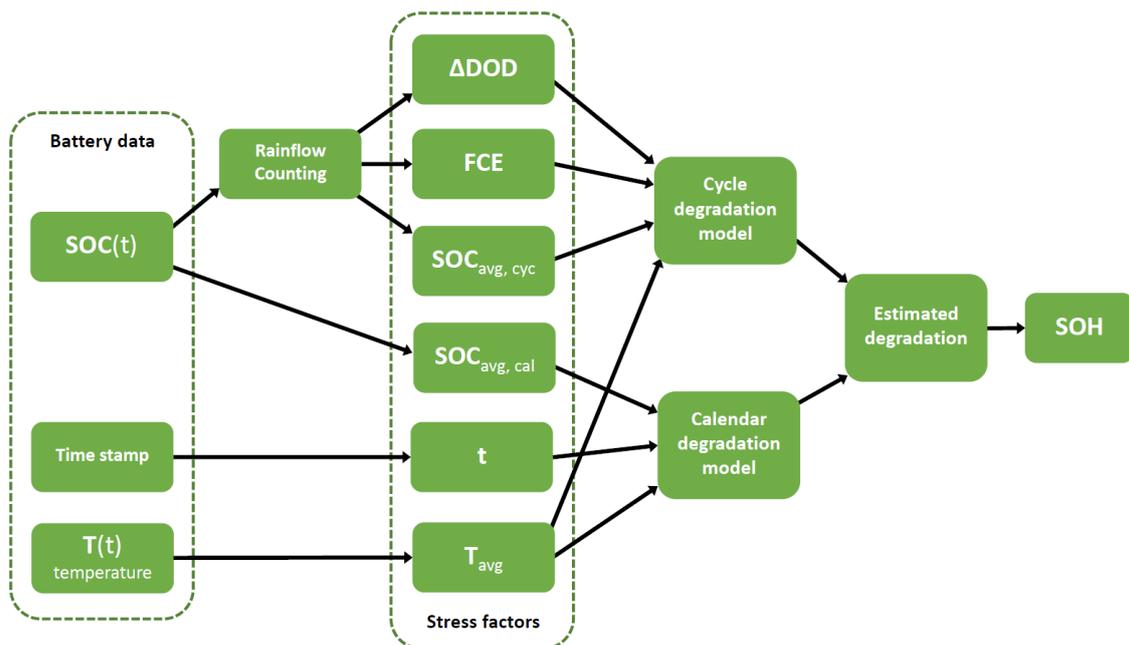
Figure 16: The operating principle of the degradation model.

The cycle degradation model estimates the capacity degradation occurring due to the operation of the battery. The cycle degradation model takes into account four degradation stress factors related to cycle aging: cycle depth (ΔDOD), average SOC during cycling ($SOC_{avg,cyc}$), average temperature (T_{avg}) and the number of cycles cycled in full cycle equivalents (FCE) during the observation period. Cycle depths, average SOC of the cycles and number of full cycles are obtained from the SOC time series data

utilizing Rainflow Counting algorithm. The Rainflow Counting algorithm is a generic cycle counting technique traditionally used for material fatigue analysis, but it has been successfully applied also for analyzing battery operation cycles [27].

The calendar degradation model estimates the capacity degradation caused by degradation processes not related to charge-discharge cycling. The calendar degradation model takes into account three degradation stress factors related to calendar aging: average SOC during storage (SOC$_{avg,cal}$), average temperature (T$_{avg}$) and time (t). The average SOC can be calculated from the SOC time series data and the average temperature from the temperature time series data.

The operating principle of the degradation model can be summarized as follows:

Estimating the degradation

1. Analyzing the SOC data with the Rainflow algorithm
   a. Calculation of cycle depths (ΔDOD)
   b. Calculation of average SOCs of the cycles (SOC$_{avg,cyc}$)
   c. Calculation of full cycles cycled during the observation period (FCE)
2. Calculation of average SOC from the SOC data (SOC$_{avg,cal}$)
3. Calculation of average temperature from the temperature data (T$_{avg}$)
4. Estimation of degradation during the observation period
   a. Estimation of cycle degradation with cycle degradation model
   b. Estimation of calendar degradation with calendar degradation model
   c. Estimated total degradation is the sum of estimated cycle degradation and estimated calendar degradation

The cycle degradation model can be expressed as:

$$
\begin{aligned}
C_{deg}^{cyc} = S_{\Delta DOD}^{cyc}(\Delta DOD, \Delta DOD_{ref}) S_{SOC}^{cyc}(SOC, SOC_{ref}) S_T^{cyc}(T, T_{ref}) C_0 \left(F_{deg}^{cyc}(FCE_0) \right. \\
\left. - F_{deg}^{cyc}(FCE_0 + FCE) \right)
\end{aligned}
$$

$$
= \frac{f_{\Delta DOD}^{cyc}(\Delta DOD_{ref})}{f_{\Delta DOD}^{cyc}(\Delta DOD)} \frac{f_{SOC}^{cyc}(SOC_{ref})}{f_{SOC}^{cyc}(SOC)} \frac{f_T^{cyc}(T_{ref})}{f_T^{cyc}(T)} C_0 \left(F_{deg}^{cyc}(FCE_0) - F_{deg}^{cyc}(FCE_0 + FCE) \right)
$$

where coefficients $S_{\Delta DOD}^{cyc}$, S_{SOC}^{cyc} and S_T^{cyc} describe the effect of each degradation stress factor on cycle degradation. These stress factor coefficients are based on the degradation stress factor models $f_{\Delta DOD}^{cyc}$, f_{SOC}^{cyc} and f_T^{cyc} formed in Chapter 3.1. C_0 is the initial capacity of the battery, F_{deg}^{cyc} is the cycle aging model for the battery, FCE_0 is the cycle age of the battery in the beginning of the observation period and FCE is the number of full cycles performed during the observation period.

An example cycle aging model for NMC cell is presented in Figure 17. The cycle aging model is based on battery lifetime data provided by the battery manufacturer and depends on battery chemistry and type. In practice the cycle aging model based on experimental cycle life data also includes the time dependent degradation (calendar aging) occurring during cycling. The cycle life tests are typically performed with higher C-rates than those used in INVADE pilots and therefore the corresponding number of cycles is achieved in shorter cycling time. If the pilot battery is operated with low C-rates it is reasonable to extend the calculation of calendar degradation to cover also the cycling phase.
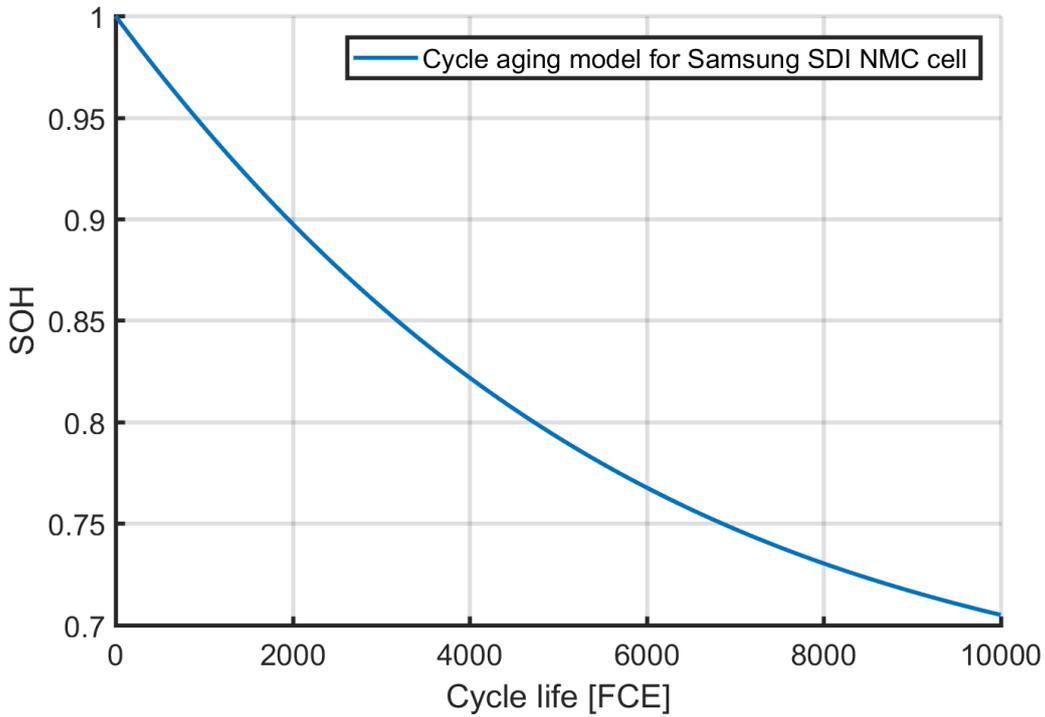
Figure 17: A cycle aging model for Samsung SDI NMC cell. The model is based on Samsung SDI's lab test results for Samsung SDI 68Ah cell presented in [25]. Test conditions: 100% DOD, 1C/1C, 25°C.

The calendar degradation model can be expressed as:

$$C_{deg}^{cal} = S_{SOC}^{cal}(SOC, SOC_{ref})S_T^{cal}(T, T_{ref})C_0\left(F_{deg}^{cal}(t_0) - F_{deg}^{cal}(t_0 + t)\right)$$

$$= \frac{f_{SOC}^{cal}(SOC_{ref})}{f_{SOC}^{cal}(SOC)}\frac{f_T^{cal}(T_{ref})}{f_T^{cal}(T)}C_0\left(F_{deg}^{cal}(t_0) - F_{deg}^{cal}(t_0 + t)\right)$$

where coefficients S_{SOC}^{cal} and S_T^{cal} describe the effects of degradation stress factors on calendar degradation. These stress factor coefficients are based on the degradation stress factor models f_{SOC}^{cal} and f_T^{cal} formed in Chapter 3.2. C_0 is the initial capacity of the battery, F_{deg}^{cal} is the calendar aging model for the battery, t_0 is the initial calendar age of

the battery and t is the length of the time period for which the calendar degradation is estimated. Time t can be either the length of the observation period or battery idle time during the observation period, depending on how the cycle aging model and calendar aging model are implemented. A linear calendar aging model based on reported battery calendar life is used unless better information is available.

The total degradation is the sum of estimated cycle degradation and estimated calendar degradation:

$$C_{deg} = C_{deg}^{cyc} + C_{deg}^{cal}$$

The degradation stress factor models as well as the cycle aging model and the calendar aging model depend on the chemistry and type of the battery. Therefore, the degradation model needs to be customized according to the battery to be modelled.

5.2   Implementation of the SOH estimation tool

The SOH estimation tool is implemented as a stand-alone tool, which can be used to update the estimated SOH of the battery for the INVADE platform. The tool incorporates a battery degradation model (Chapter 5.1) that addresses the degradation stress factors to the historical usage data of the battery system. Time-series data is given as an input, and the estimated SOH is provided as an output. As the change of the battery SOH is slow, a periodic update of the SOH estimation in the platform is enough to maintain sufficient accuracy in battery state estimation.

The SOH tool is implemented on Microsoft Excel so that its use would be simple for the INVADE pilots. For estimating the battery SOH, the Excel based SOH tool requires some basic battery parameters and measurement data from the pilot battery. Required inputs for the SOH estimation tool are presented in Table 9.

Input	Symbol	Unit	Explanation
Nominal capacity	C_{nom}	kWh	The nominal capacity of the battery.
Initial capacity	C_0	kWh	The capacity of the battery at the beginning of the observation period. Can be calculated from nominal capacity if the initial SOH is known.
Initial calendar age	t_0	day	The calendar age of the battery at the beginning of the observation period.
Initial cycle age	FCE_0	FCE	Number of cycles cycled at the beginning of the observation period.
SOC	SOC	%	Battery SOC time series data during the observation period.
Battery temperature	T	°C	Battery temperature time series data during the observation period. Environmental temperature can be used if no temperature data from battery pack is available.

Table 9: Required inputs for the SOH estimation tool.

The most important measurement data is the SOC of the battery during the observation period. Sufficient measurement frequency would be the same as in the INVADE platform, which is every 15 minutes. Another useful measurement data is the temperature of the battery during the observation period. Environmental temperature or longer-term average can also be used if no temperature data measured from the battery pack is available.

To use the SOH estimation tool, basic battery parameters (Table 9) and time series data from the battery need to be imported to the Excel-based tool. The data should include the SOC value and corresponding time stamp throughout the whole observation period. Also temperature data should be included if it is available. Once the data is imported, the Rainflow Counting algorithm and other algorithms implemented in Excel analyse the historical data and identify the stress factor conditions.

The degradation model (Chapter 5.1) implemented in Excel takes into account these stress factor conditions and estimates the cycle degradation and calendar degradation of the battery during the observation period. Based on these estimates and the nominal capacity (C_{nom}) and the initial capacity of the battery at the beginning of the observation period (C_0), the SOH tool calculates the estimates for the current capacity and SOH of the battery. A development version of the SOH estimation tool is presented in Figure 18.
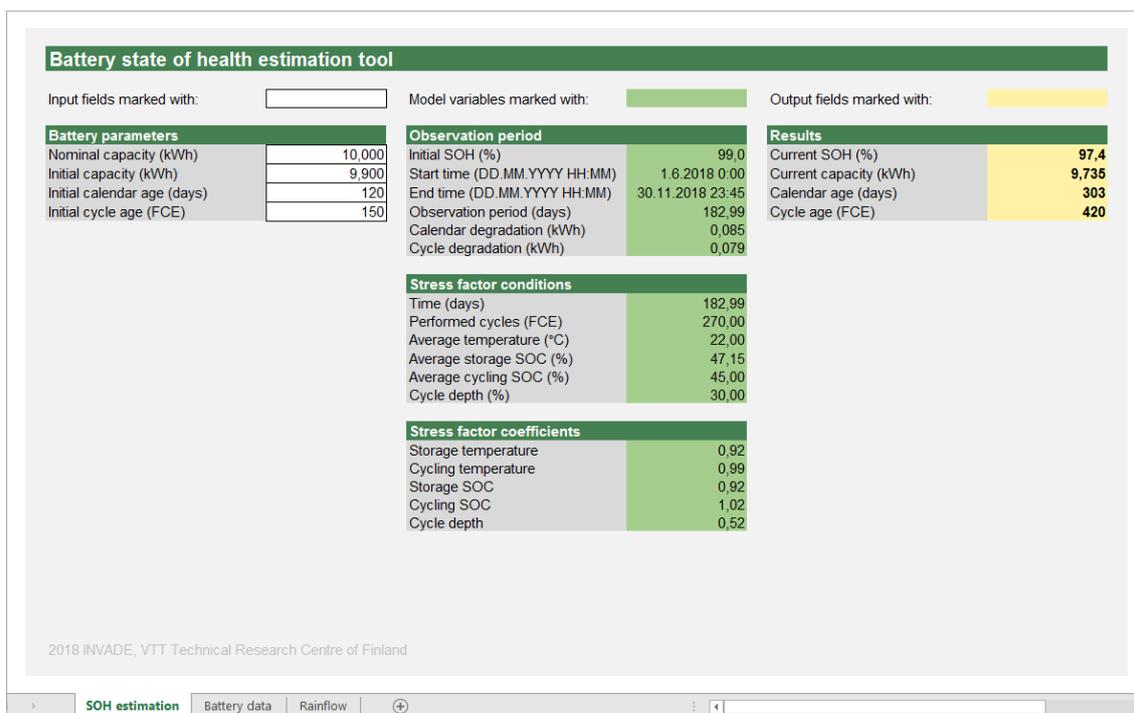
Figure 18: A development version of the SOH estimation tool implemented in Excel.

For different INVADE pilots the SOH estimation tool needs to be customized depending on the battery used in the pilot. The degradation model integrated into the SOH tool utilizes different degradation stress factor models depending on the battery chemistry. Additionally, the degradation model exploits the lifetime data provided by the battery manufacturer, which depends on the battery type.

6 Battery end of life criteria

When the battery can no longer meet its performance requirements, it has reached its end-of-life (EOL), and has to be removed from the application. Being able to properly define this point is important, because it affects both the system performance and safety. If the battery has degraded too much, it may not be able to respond to the requirements set by the application where the battery is used. Also the risk of a critical failure happening in the battery pack will increase when the battery degrades. Earlier, we have explained that EOL is typically defined to be reached when the capacity of the LIB has decreased to 80% of the rated capacity [1].

For electric vehicle (EV) batteries a typical definition for end-of-life is when 70-80% of the original energy capacity is remaining [28] [29]. This originates to a standard established by the US Advanced Battery Consortium (USABC) in 1996. According to this standard the EOL has been reached when either the net delivered capacity of a cell, module or battery is less than 80% of its rated capacity or the peak power capability is less than 80% of the rated power at 80% DOD [30]. After that, several other standards have been published regarding EV LIBs, e.g. IEC 62660-1:2010, ISO 12405-4:2018, and SAE J2288:2008, shown in Table 10. A review on the existing and upcoming standards has been published by JRC [31].

Naturally, one key issue when determining the EOL is the durability of the battery. Over its lifetime, the performance of the battery deteriorates due to the effect of both electrochemical ageing during usage and calendar ageing when not being used. The factors affecting to this ageing have been discussed already in D6.3 [1] and in Chapter 3. For EV batteries, various lifetime targets have been set: A calendar life of 10-15 years by 2020 and 2000-3000 discharge cycles was set by U.S. Department of Energy [31], and lifetime of 10-15 years by 2030 was set in the EUROBAT's roadmap [32]. One challenge is that the lifetime results vary a lot depending the chemistry and even between different cells with the same chemistry.

Four types of testing methods for EOL are presented in current standards. Calendar ageing tests are used to measure the battery performance (e.g. capacity) under a defined temperature during a defined period of time. Cycle life ageing tests are used to measure the performance parameters as a function of cycle number during electrochemical cycling at a defined temperature, current rate, and upper and lower cut-off voltages. In-vehicle ageing tests are used to measure the battery performance under real driving conditions by using a driving cycle, e.g. New European Driving Cycle (NEDC). In an

accelerated ageing test, a battery cell is aged by enhancing the rate of degradation process compared to normal operation. Functional parameters, e.g. capacity, internal resistance, etc. are measured. The purpose of the accelerated ageing test is to reduce the amount of time used in the testing. However, reaction path should remain the same as in the normal ageing, otherwise, the result may not be correctly extrapolated to normal ageing conditions. It is worth noticing that none of the existing standards combine the effect of cycle ageing and calendar ageing. [31]

Cycle life standards consist of methods to determine initial performance of the battery, used charge/discharge cycles, methods to periodically evaluate the battery performance during cycling, and termination criteria for the cycle life test. European standards concerning the cycle ageing are IEC 62660-1:2010, ISO 12405-4:2018, SAE J2288:2008, and SAE J1798:2008. Both IEC and ISO standards have different requirements for HEVs and BEVs. One question regarding the cycle life standards is whether the cycle tests should be performed in cell level or system level. Currently, the ISO 12405 standard requires tests in system level while, the in the IEC 62660 standard, the tests are done in the cell level. In SAE 2288:2008, the tests are done in module level. [31]

Both IEC 62660-1:2010 and ISO 12405-4:2018 require different test conditions for HEV and BEV batteries. For the capacity determination, constant current cycling at 1/3C is required for BEV batteries and 1C for HEV batteries. HEV batteries should be tested between 30% and 80% SOC whereas for BEV batteries the test region is between 20% and 80% SOC. [31]

Regading cycling, one difference is the temperature. The IEC 62660-1:2010 requires cycling at 45 °C, and the performance evaluation at 25° for both BEVs and HEVs, whereas ISO 12405-4:2018 requires 25 °C temperature for HEVs and for BEVs the cycling is performed at 25°C and the performance evaluation is done in both 25°C and -10°C. SAE J2288:2008 requires all testing done in 25 °C. [31]

SAE J2288:2008 defines a test methodology to determine the expected service life of electric vehicle battery modules. The performance of the module is checked every 28 days of cycling. The performance parameters and periodic performance evaluation is similar to that in IEC 62660.1:2010.

In most standards, the termination criteria for the cycle age test is that if one of the performance values have decreased below 80% of its initial value, the test is terminated. The exception is ISO 12405-4:2018, which only requires to report the decrease of the capacity but does not require to terminate the test. [31]

Table 10. Standards regarding the EOL and cycle life of EV batteries.

Standard	Level	Performance measurements measure	Termination
IEC 62660	cell	HEVs: capacity every 14 days power every 7 days BEVs: every 28 days, measure capacity, dynamic capacity (25°C and 45°C) and power at 50% SoC in 25 °C	if capacity, dynamic discharge capacity or power has decreased to less than 80% of the initial value (BEV) if capacity or power has decreased to less than 80% of the initial value (HEV)
ISO 12405-4:2018	system	HEVs: power test after 7 days capacity every 14 days BEVs: every 28 days perform standard cycle and charge every 8 weeks	limits defined by manufacturer reached power test cannot be performed fully agreement between supplier and customer
SAE 2288:2008	module	capacity, dynamic capacity, power every 28 days	measured capacity is <80% of the rated capacity peak power capability is <80% of the rated power at 80% DoD

6.1   Second life batteries

In 2018, European Union published a JRC report on Standards for the performance and durability assessment of electric vehicle batteries. One of the outcomes of this report was concerning second life batteries:

"*A clear definition of battery end of life (EoL) is needed. There is a need for establishing standards containing criteria and guidelines for evaluating battery status (e.g. state of health (SoH), safety) and its potential usefulness for second use applications.*" [31]

There are not many publications related to EoL or SoH of second life batteries. However, a literature review by Martinez-Laserna et al. found out that in many publications it has been shown that batteries reaching the ageing knee would not be eligible for a second life use [33]. For example, in a study by Martinez-Laserna et al. battery second life ageing performance was analysed with cells at different ageing phases. Those cells which were reused on a second life application before reaching the ageing knee (i.e. before experiencing a change in the dominant ageing mechanism), showed very good performance. The cells that were reused after reaching the ageing knee exhibited a very fast degradation. [34] In another experimental study by Martinez-Laserna et al. data proved that reusing the batteries on a mild demanding application does not slow down the ageing trend, once the ageing knee is reached. Thus, according to the results, the cells experiencing any changes in the dominant ageing mechanism would have to be retired from operation, either on the first or the second life use phases, because of two main reasons:

1. Ah-throughput (and thus the number of cycles) that these cells can withstand after reaching the ageing knee would be insufficient to make profitable extending their operation

2. It might be unsafe to maintain such cells in operation.

To conclude, only the cells that do not experience any changes in the dominant ageing mechanism may be eligible for a second life use. [35]

Additionally, since the dominant ageing mechanism would not change before retiring the batteries from operation, there would not be any electrochemical difference in the batteries' ageing phenomena, and hence first life battery lifetime models might be also usable to predict the second life battery ageing performance. Taking into account the strong influence of the first life battery ageing upon the technical viability of a potential second life use, tracking data of first life battery ageing appears as a key resource for

decision making. Indeed, the first life battery ageing data would be crucial to select the most suitable batteries and predict their ageing performance on a potential second life use. Similarly, tracking second life battery ageing turns out to be essential to identify battery failure and avoid any safety events. [35]
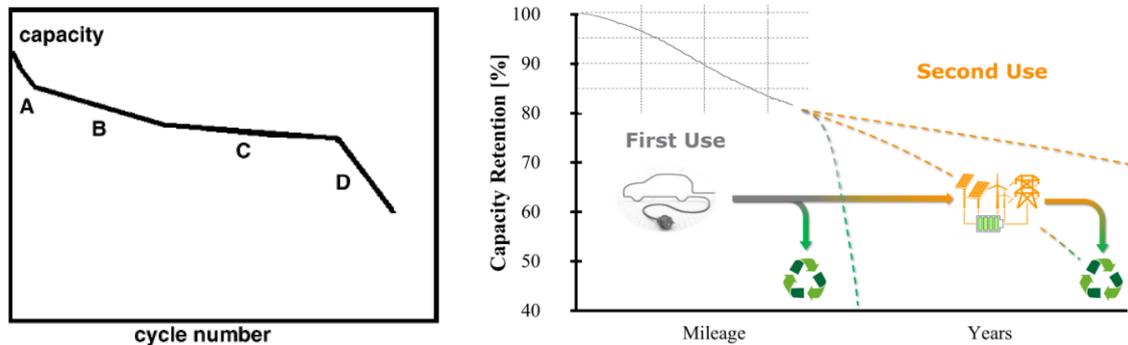

Figure 19. Left: General shape for capacity versus cycle number plots [36]. Right: Capacity retention with First Use mileage and Second Use duration [37].

Figure 19 highlights the features of a very general capacity versus cycle number plot. The shape is reminiscent of a discharge curve (voltage versus capacity), and necessarily so. The rate of capacity decrease is initially high (region A), but slows quickly (region B) and, after a few hundreds of cycles, slows again (region C) before starting a rapid increase (region D). End of life, defined as when the battery reaches 80% of its initial capacity, usually occurs in region C, so battery manufacturers do not publicly report data for region D. [36]

The following summary of experimental data can be made [36]:

1. Capacity loss on storage has reversible and irreversible components.
2. Capacity loss on storage or cycling increases with increasing temperature.
3. Capacity loss on storage increases with increasing cell voltage.
4. Cycling causes capacity loss at a greater rate than storage.
5. Capacity loss can correlate with cell impedance.

It is crucial to be able to observe the ageing knee. This could be done by monitoring and logging SOH over the use. At the linear phase of the capacity vs. cycle number (time) the slope (s) is k. As soon as the slope changes dramatically (s<<k) it can be stated that the ageing knee has been reached. In order to be able to define the right values for linear phase (k) and ageing knee, the following knowledge is required:

1. Usage/ageing history in the first life.
2. Point of retirement in the first life.
3. Requirements of the second life applications.

7 Screening life cycle assessment of batteries

The screening LCA study in INVADE focuses on defining the assessment framework and finding the best available estimates for the global warming potential of batteries applied in the pilot sites. The intention of this study is not to cross-compare the pilots or various battery technologies used within the project, but rather to assess the environmental benefits associated with the implementation of the pilots. One of the key benefits of life cycle thinking is avoidance of environmental burden shifting across multiple life cycle phases. This means that impacts at one specific phase of the life cycle cannot be minimized at the cost of increased impact in any other phase.

The batteries with specifications presented in Table 1 have been and will be further studied in this project. The research work included also personal contacts to pilot representatives and other technology experts to find out the status and technical specifications for pilots. The screening LCA serves as a basis for the full scale LCA to be performed further using the field data from the pilots.

7.1 Methodological background

As depicted in Figure 20, the life cycle of a battery begins from the raw material extraction and conversion, continues to production, distribution and use. The life cycle ends with so called end-of-life phase. With the growing emphasis on circular economy, the re-use of batteries, remanufacturing of its elements, and recycling or recovery of materials should be prioritized over conventionally practiced landfill disposal.
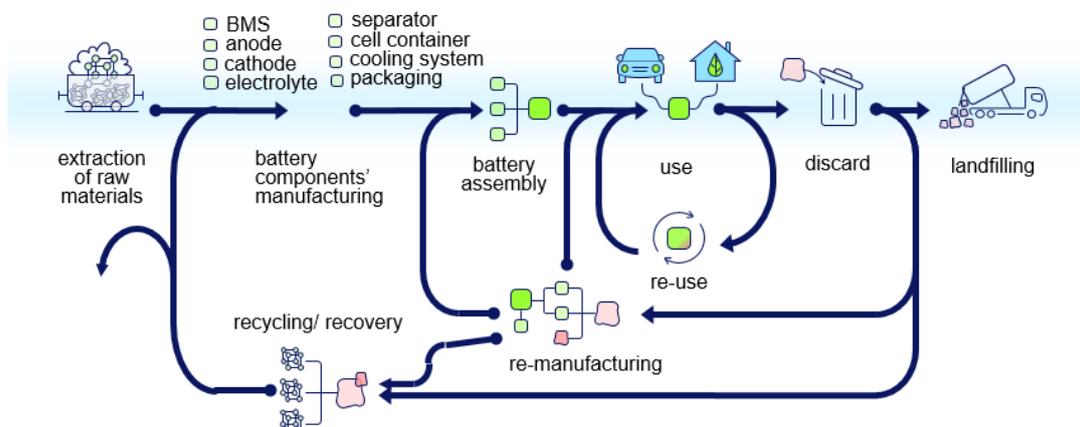

Figure 20. Battery life cycle [38]

Despite screening LCA does not have its own methodology per se, it predominantly follows the LCA methodology presented in international ISO 14040/44 standards. A

typical LCA included four phases: goal and scope definition, inventory analysis, impact assessment and interpretation. First in LCA the goal and the scope are defined. The inventory analysis denotes for the input data collection. The input data for LCA is either primary or case-specific, i.e. originating from the actual production processes, or secondary or average, i.e. collected from generic databases and literature. Data collection questionnaire is a common way to collect data from suppliers in an LCA. In INVADE, an Excel based screening LCA questionnaire (Figure 22) was created and tailored for each pilot depending on its specifications. In this study, the screening approach referred to limited data collection as compared with the full scale LCA and reported the available results per one part of the studied system, e.g. battery production. The relation between the inventory and impact assessment phases is shown in Figure 21.
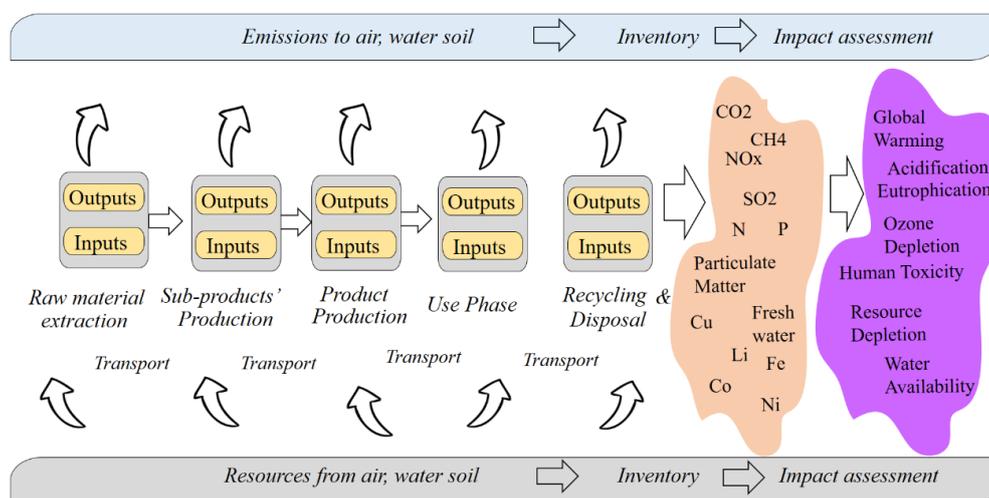
Figure 21. The inventory and impact assessment phases in LCA

QUESTIONNAIRE FOR INVADE LIFE CYCLE ASSESSMENT (LCA)
UPC - 03.10.2018

1. DOCUMENTATION
Pilot Site Name
Country
Contact person
E-mail
Date

Leave empty rows if no data is required
2. PILOT SITE INFORMATION *(Add rows if needed)*

Units (change and highlight if needed)

Customers

PV		
Units		no.
Manufacturer		
Model		-
Cell type		Monocrystalline/Polycrystalline
Peak Power		kWp
Area		m2 (PV panel area)
number of cells		no.

Storage (new)		
Manufacturer		-
Model		-
Units		no.
Energy		kWh kW max control (peak-shaving)

controllable Loads		
Water Boilers		units
Peak Power		kW
Water capacity		m3
Water capacity		m3

Storage (2nd Life)		
Manufacturer		-
Model		-
Units		no.
Energy		kWh

Local controller		
model		(average model)
manufacturer		kW

Figure 22. Screening LCA data collection questionnaire

As a results of the inventory analysis, a list of emissions, wastes and raw materials from the whole life cycle of product is being compiled with their amounts. This step is carried out in LCA tools.

In the impact assessment stage, the results from the inventory stage are classified into selected environmental impact categories as shown in Figure 23 with the example of several emissions for global warming, acidification, and abiotic depletion impact categories. Finally, the masses of emissions and raw materials are multiplied with

specific factors to get the results in equivalents of reference substances, e.g. carbon dioxide for the global warming category. The characterized results could complementary be normalised and weighted. Commonly, the impact assessment is carried out with an LCA software tool.
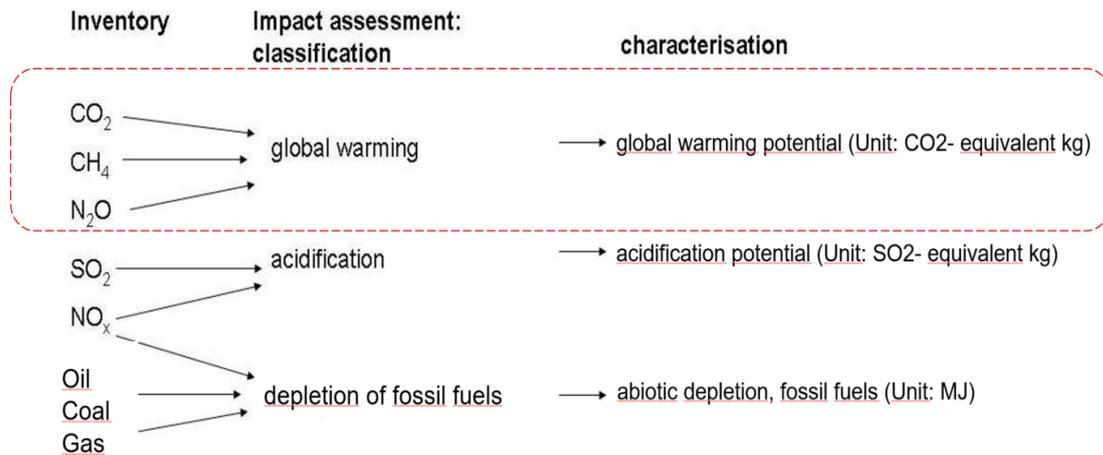

Figure 23. Framework of the impact assessment steps for three different impact categories, global warming potential highlighted

The tools used in this study are SULCA and GaBi. The databases used are those provided by GaBi and Ecoinvent [39]. Some information was sourced from literature. The related characterization factors are employed at the midpoint level, i.e. without normalisation and weighting. Environmental impact was limited to the impact on climate change only. Other impact categories which could be included if sufficient data is available include ozone depletion, photochemical ozone creation, terrestrial acidification, marine eutrophication and fresh water eutrophication.

Finally, the results of the LCA study are summarized during the interpretation stage. Also, relevant conclusions taking into consideration the objectives set and the wanted use purpose are being made. The interpretation means in this study that the authors recommend next steps to the full-scale LCA.

7.2 Li-ion batteries

The main components of a Li-ion cell are anode (negative electrode), cathode (positive electrode), electrolyte and a separator between them. The structure of a Li-ion cell is presented in Figure 24. In applications, such as EVs, the battery cells are assembled into larger units called battery modules, which form the battery pack. In addition to the battery cells, the battery pack contains also a cooling system and a battery management system (BMS), which controls the use of the battery pack and monitors the state of the cells.
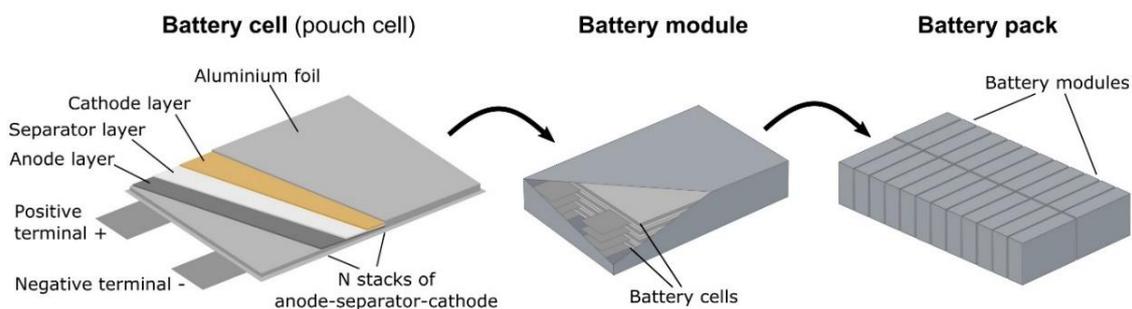
Figure 24. Structure of a Li-ion cell and battery pack. [38]

The environmental impact of batteries was assessed analysing the available data and studies. In the literature there are LCA studies on several battery types. Following the needs of the INVADE pilots, only LIBs with NCM and LFP chemistries, as well as redox flow batteries, were analysed. No other types of batteries were studied.

Peters and Weil [40] identified five studies with complete and sufficient life cycle inventory on the production of LIBs including the studies by Majeau-Bettez et al. [41] and Ellingsen et al. [42]. All relevant articles were brought to a shared library kept in Mendeley. The inventory from Majeau-Bettez et al. [41] and Ellingsen et al. [42] was replicated in the project using LCA software tool SULCA and the Ecoinvent v3.4 database. The LCA model created after Majeau-Bettez et al. [41] for NCM and LFP batteries is presented in Figure 25. The model allows to change some of the parameters of the battery production and assembly process. Replication of the model enables deeper analysis of environmental impact of the batteries. The contribution of different processes to the environmental impact of the NCM battery modelled after Majeau-Bettez et al. [41] is shown in Figure 26. The results showed that the battery production and assembly, production of BMS and positive electrode production are the main contributors to this results.
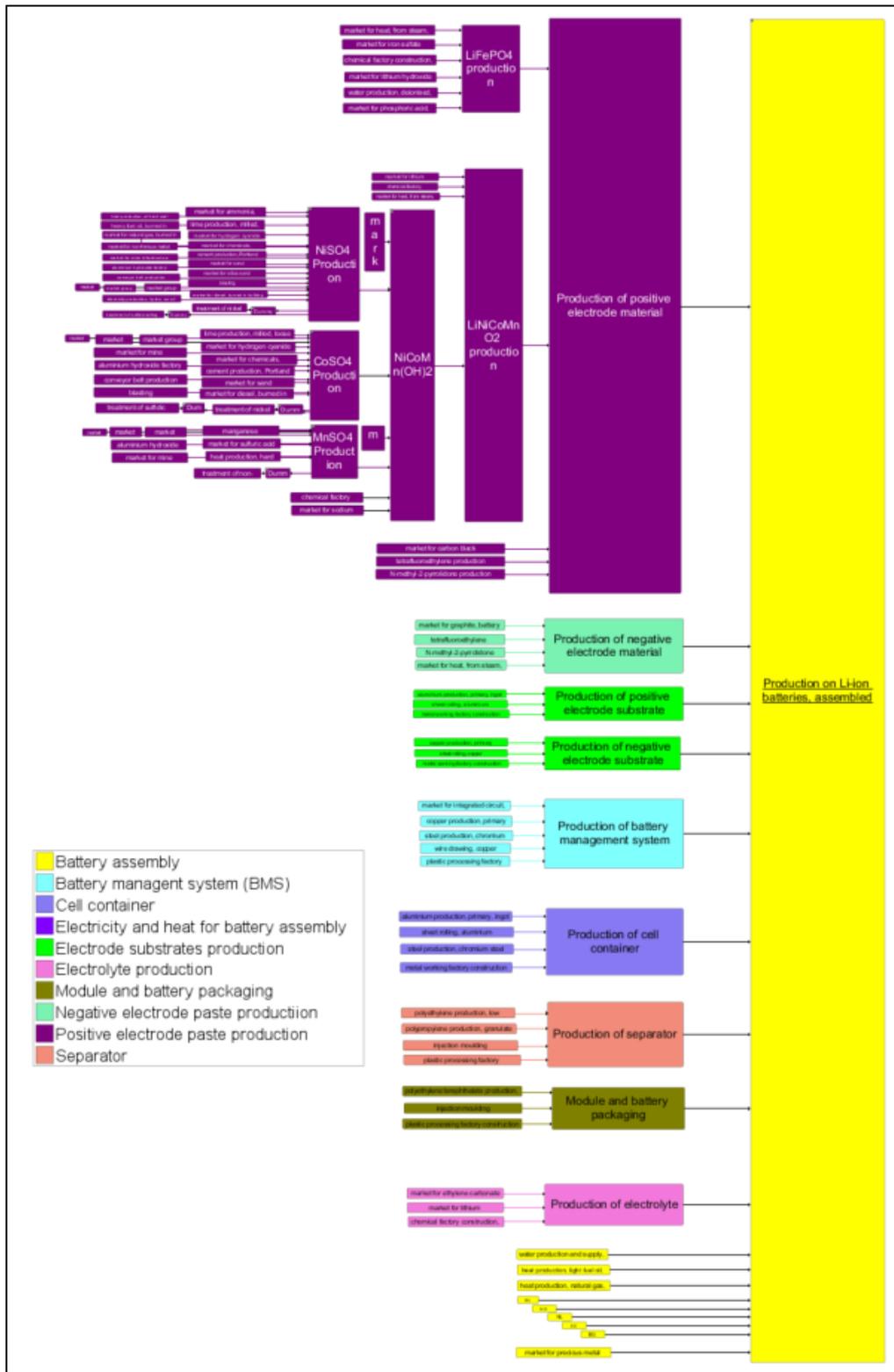
Figure 25. SULCA modelling flow sheet for NCM and LFP li-ion battery modelled after Majeau-Bettez et al. [41]
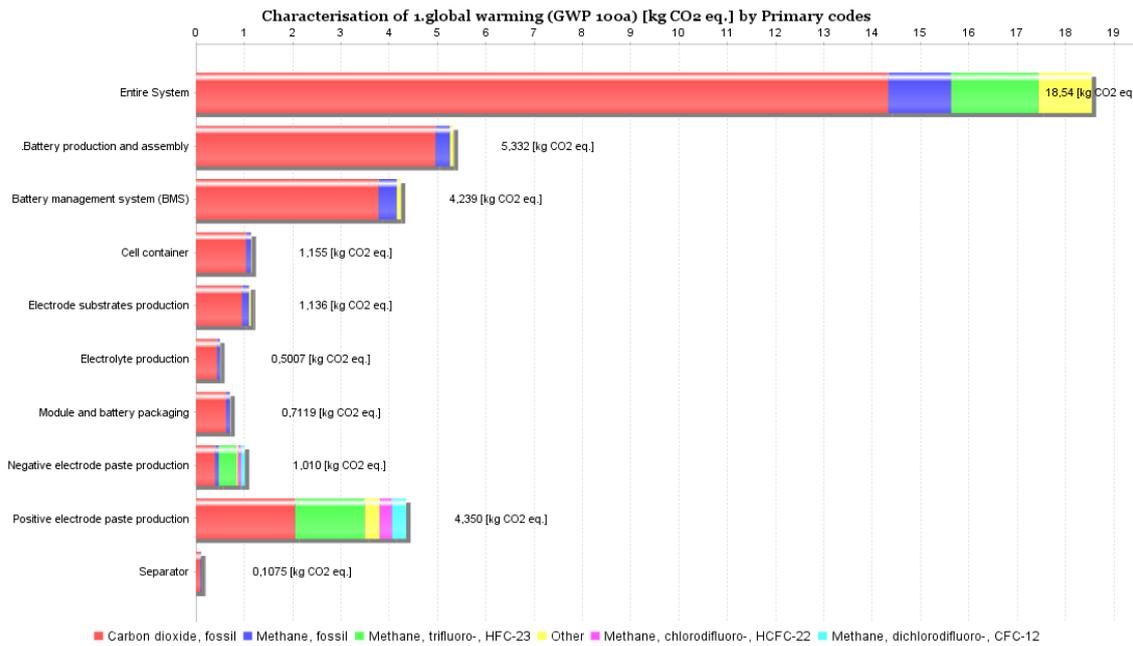
Figure 26: The cradle-to-gate GWP and the GWPs of battery components indicators per kg of Li-ion battery (NCM)

Table 11 lists the GWP values of NCM batteries production retrieved from literature for comparison. The values are presented per kWh of storage capacity of the battery.

Table 11. GWP values from selected studies for NCM batteries

Literature source	GWP, kg CO_2-eq/ kWh storage capacity	Which life cycle stages included	Notes
Ellingsen et al 2014 [42]	172; 240-487	cradle-to-gate	The lower value gained under the optimal conditions, whereas the higher range reported depending on the amount of electricity consumed during the batteries production
Ambrose and Kendall 2016 [43]	254	cradle-to-gate	Mean GWP
Kim et al 2016 [44]	140	cradle-to-gate	
Majeau-Bettez et al., 2011 [41]	200	cradle-to-gate	
US. EPA 2013 [45]	121	cradle-to-gate	producing 1kWh of storage capacity

7.2.1 Use in stationary applications

When LIBs are used in stationary applications, they can be used to increase the utilization rate of renewable electricity produced from solar panels of wind farms and thus to reduce the impact from consuming grid electricity.

The value of GWP in the use phase depends on the energy grid mix. Table 12 summarizes the GWPs for country specific electricity grid mixes. The value "GWP, solar" refers to the GWP of solar electricity generation accounting for the impact from solar panels production and the use of water for washing the panels during their use phase and wastewater treatment. The value "GWP, average" relates to the average GWP values retrieved from the Ecoinvent database and from Moro and Lonza [46]. Furthermore, using the historical data of the share of renewables in the electricity grids in chosen countries retrieved from World Bank [47] (Figure 27), the share of renewables was extrapolated to the year 2025 to make up the column "GWP, in 2025".

Table 12. GWP values for country-specific grid mixes, according to Ecoinvent 3.4 database

Country	GWP, solar, g CO_2-eq/ kWh	GWP, average, g CO_2-eq/ kWh	GWP, in 2025, g CO2-eq/ kWh
Germany	102	622	N.A.
Bulgaria	71	656	560
Spain	65	347	242
the Netherlands	98	558	507
Norway	80	21	not listed due to currently high share of renewables

N.A. - not analysed because the information on the German pilot plant came after the analysis have been performed.

It shall be noted that the local grid mix and the mix during peak hours might differ substantially. As the batteries are applied to peak shaving during peak hours, the impact during the peak hours is more relevant for the project than the average national gird mixes. The local grid mixes are analysed in INVADE by UPC and reported in D3.4 *Draft life cycle analysis*.
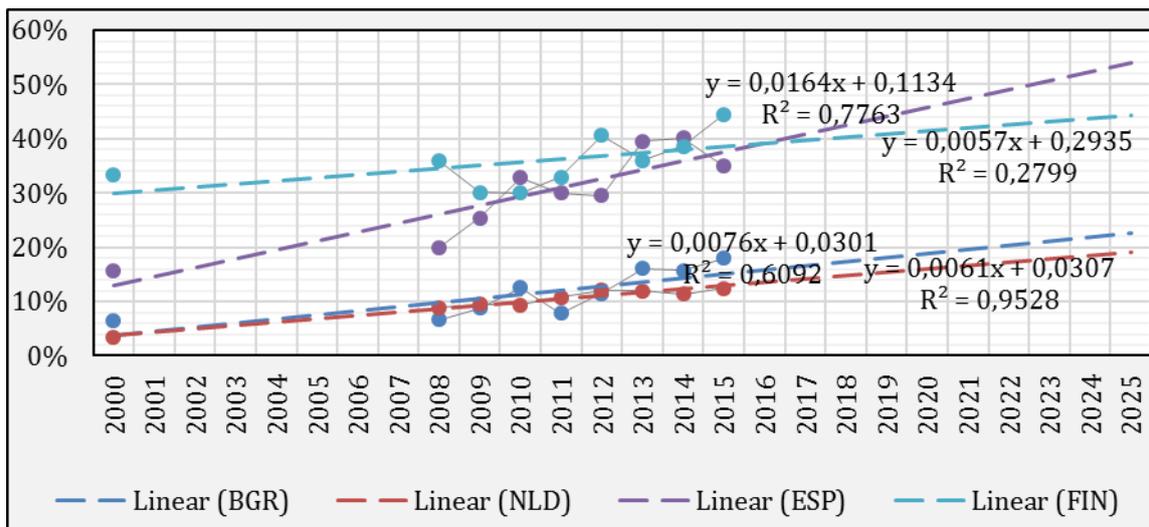
Figure 27: Share of renewable electricity in chosen countries (World Bank 2018) *and predictions based on a linear correlation*

7.2.2 Recycling

There are multiple options for recycling of LIBs. According to Zeng et al. [48], all LIBs recycling processes could be divided into mechanical, pyrometallurgical, hydrometallurgical, and biological. According to the authors, research on hydrometallurgical recycling of LIBs occupies 58% of all research activities in the field. During the process, LIBs are dismantled into different parts, and then metal-containing fractions incinerated and slag is leached with chemicals to selectively regain metals.

As with the LIBs production, data on LIBs recycling is uncertain. The following values for recycling of LIBs are listed in the table. The median GWP value from these sources identified was 16±11 kg CO2-eq./ kWh.

Table 13. GWP values from selected studies for LIBs

Literature source	GWP kg CO_2-eq/ kWh	Which life cycle stages included
Ellingsen et al 2016 [49]	8	recycling
Li et al 2014 [50]	27	recycling
US. EPA 2013 [45]	16-32	recycling

7.2.3   Remanufacturing

Besides recycling, the batteries can be refurbished to fulfil the needs of other applications, so called second-life applications. This is particularly possibly for the batteries used in vehicles because they still have approximately 80% of their capacity at the end of their service. Usually, batteries which reached their end of their service lives are being transported to the remanufacturing facilities where they are inspected and tested to determine the SOH. If needed, the container, battery management system, and other auxiliary components of the batteries could be replaced. Due to their less-demanding use in stationary applications, the second-life BMS systems are smaller and lighter compared to an EV's BMS [51]. The energy consumption of the remanufacturing is estimated as the level of 27 kWh per battery check [52] or 4812 kWh for testing 4500 cells from EV LIB packs to build one stationary battery pack for 450 kWh energy storage [51].

7.3   Calculation results from degradation stress factor analysis

To study the integration of degradation stress factors within LCA, NCM batteries made by Nissan (Gen4) and installed in a Norwegian pilot plant were used as a point of reference. Table 14 lists the specifications of the batteries used in this LCA study. The warranty conditions imply the use of the battery for 2810 cycles, which would mean its use for 7,7 years with 1 cycle per day and the energy throughout of 25,3 MWh. The reference conditions for the lifetime determination were: 90% cycle depth, 50% average state of charge, operating temperature of 25 ºC.

Table 14: Parameters of batteries used in the LCA study incorporating stress factors.

Parameters	Value
Cell chemistry technology	NMC
Nominal capacity	10 kWh
Ah per pack	111,4 Ah
Warranty (daily, 90%DoD, 1C)	313000 Ah
Initial SOH	100%
Roundtrip efficiency	90%

Figure 28 shows that consuming 25,3 MWh of electricity from grid in Spain during the lifetime of the battery would results in emitting 8760 kg CO2-eq., whereas installing a battery with 10 kWh capacity, daily using it and terminating would result in the GWP of 3520 kg CO2-eq. This means that a 60% reduction from the baseline situation could be achieved. This reduction for other countries studied, namely Bulgaria, Finland, the Netherlands, and Norway ranged 0-78%.
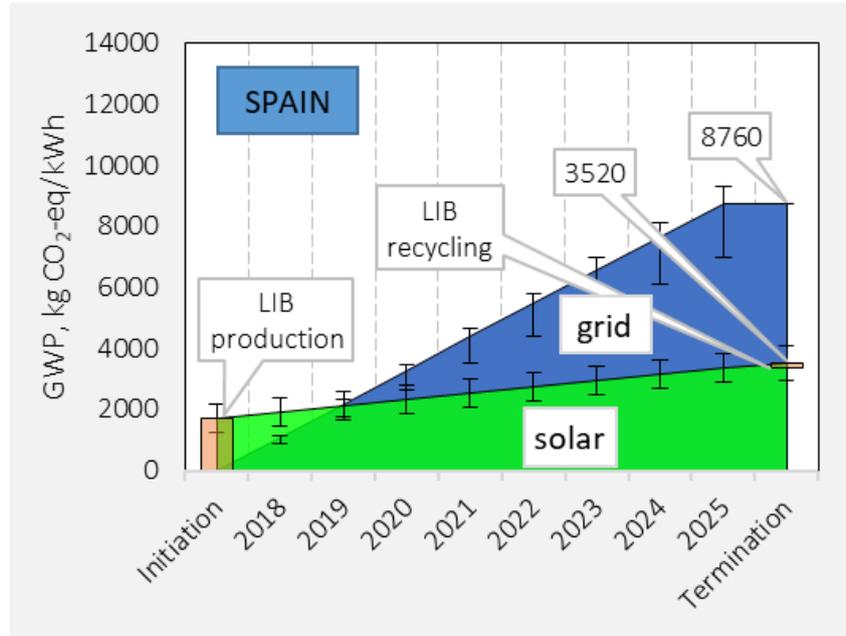

Figure 28: GWP of using electricity from existing grid (blue area) and that of using electricity from solar panels and stored in batteries installed on that purpose and terminated after the lifetime of the battery.

When considering the impact of stress factors on lifetime of the battery, which was described previously, the following situation were studied:

1. decrease of depth of discharge from 90% to 50% (S1) resulting in the increase of the energy throughout to 56,9 MWh;

2. increase of operating temperature from 25 ºC to 40 ºC (S2.1) or decrease to 10 ºC (S2.2) resulting in the decrease of the energy throughput to 13,7 MWh and 17,7 MWh, respectively;

3. increase of the average state of charge from 50% to 75% (S3.1) and decrease to 25% (S3.2) resulting in the decrease of the energy throughput of 11,8 MWh and 14,3 MWh, respectively.
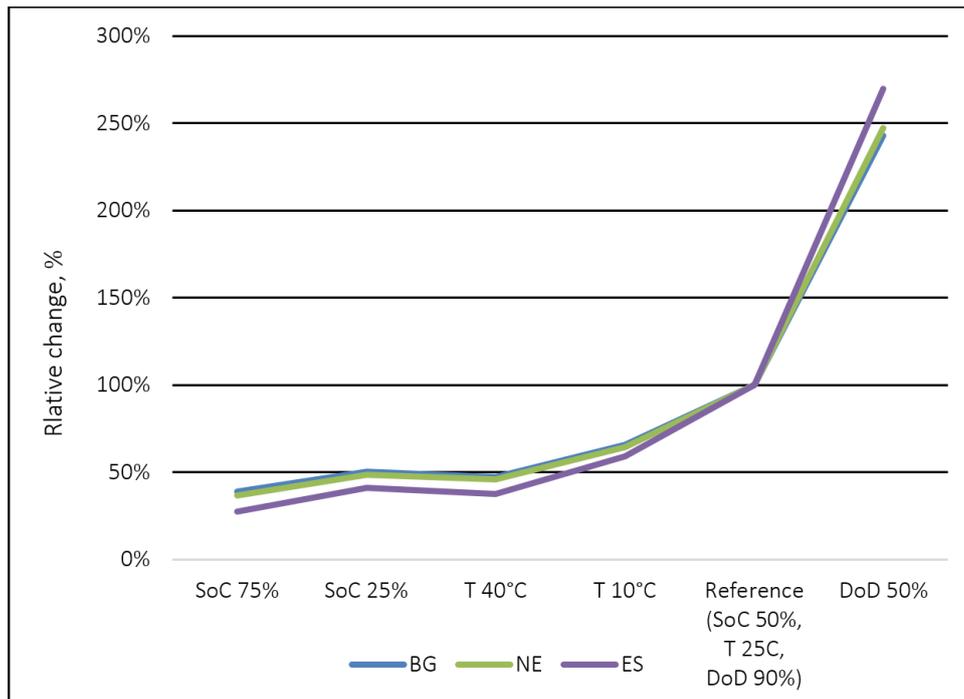
Figure 29: Comparison of the influence of different impact factors on the results for different countries (BG - Bulgaria, NE - the Netherlands, ES - Spain).

Figure 29 shows that the decrease of the depth of discharge is the only stress factor resulting in prolonged battery lifetime. The reduction of the depth of discharge to 50% significantly prolongs the lifetime of LIBs by around 2,5 times, which in turn results in higher GWP reduction as compared to the reference scenario of battery use. It should be noted that the impact of the depth of discharge on the battery's lifetime was modelled using the findings of Ecker et al. 2014 [4] which are presented in Figure 2. The findings show dramatic increase in the lifetime of LIBs with the reduced depth of discharge.

Other stress factors, such as the operating temperature and average SOC were the most optimal in the reference conditions, so their variation to either side resulted in reduced lifetime of the battery. Decrease of the operating temperature to 10 ºC resulted in the reduction of GWP by around 60%, while the increase to 40 ºC led to the reduction by around 45%. Finally, the decrease of the average SOC to 25% would lead to the reduction of the lifetime by around 50%, whereas the increase of state of charge to 75% would lead to the increase in the lifetime by around 35% as compared with the reference scenario.

7.4   Summary of redox flow batteries LCA results

In a redox flow battery (RFB) the energy storage and energy conversion function are separated. The liquid electrolytes are stored in tanks, and pumped through stacks of battery cells, where the electrochemical reactions take place (Figure 30). Compared to other battery types, the possibility for spatial separation gives redox flow batteries the benefit that the stacks (determinant for the power rating of the battery) and the tanks (determinant for the storage capacity) can be dimensioned and tailored independently. [53] [54] This makes the RFBs very suitable for stationary large-scale storage systems. The RFBs are gaining growing attention, due this flexible modular design and other benefits, such as long cycling life, active thermal management, and better ensured security [54].
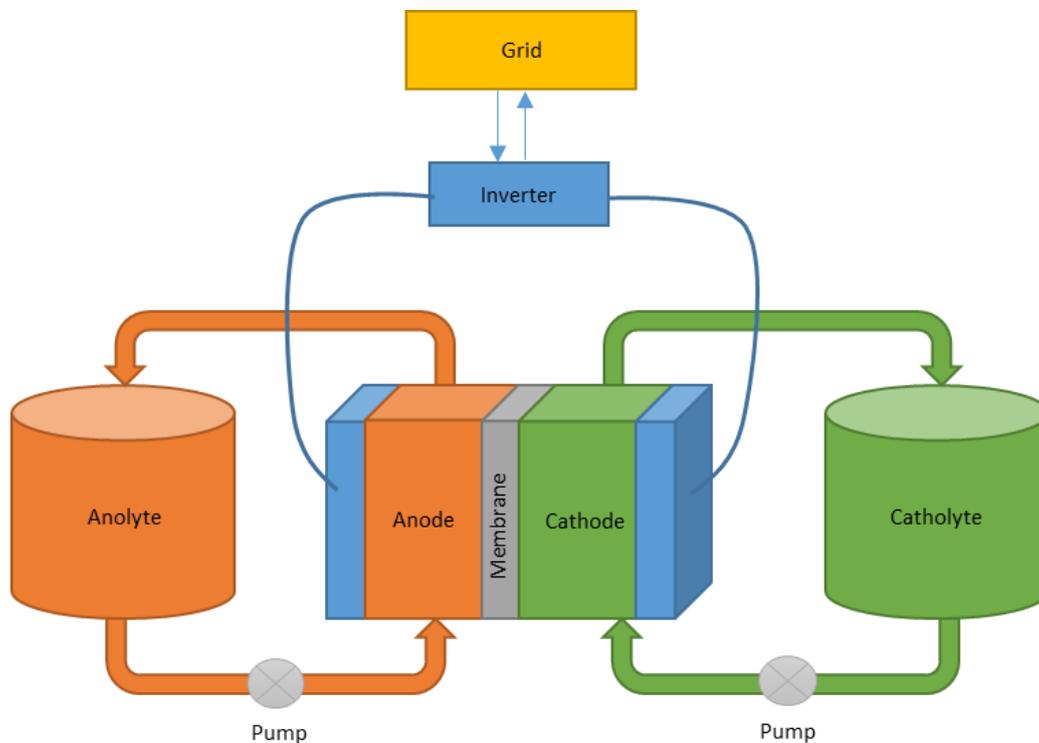
Figure 30: Basic concept of vanadium redox flow battery.

Currently, the most promising RFB technology is vanadium redox flow batteries (VRFB), where vanadium is used in the electrolyte [53]. The advantage of VRFB is that the same element can be used on both sides of the battery cell, which helps to avoid the cross-contamination of the electrolytes. In addition, the VRFBs have fast response and long cycle and service life, and they do not suffer from permanent self-discharge [53].

Weber et al. [53] have made a detailed LCA study on the emissions of producing the VRFBs. Their results propose that the emissions of the production of VRFBs are mainly

formed during the production of vanadium for the electrolyte, i.e. almost 90% of the total emissions are related to this production phase (Figure 31). Vanadium is usually produced from vanadium containing titanomagnetite ore. The main product is pig iron, and vanadium is concentrated in the slag from which it is recovered. The process requires high electricity inputs [53]. In their study, Weber et al. [53] have assumed that vanadium is produced in South Africa, where the electricity is mainly produced by coal. Therefore, the emissions of electricity used for vanadium production represent 46% of total emissions of the VRFB production [53]. According to Ecoinvent 3.5 [55], the average high voltage electricity mix for South Africa has an emission factor of 1032gCO2-eq/kWh in 2014.
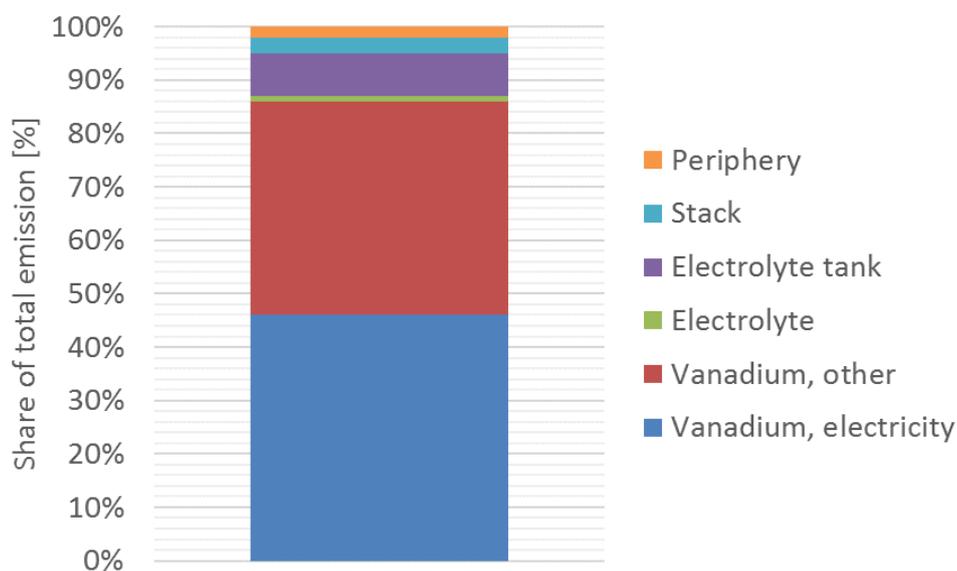

Figure 31: Illustration of the impact of the different production steps to the total emission of a VRFB. Data roughly estimated from Weber et al. [53].

Figure 32 illustrates the total emissions with possible other production sites with 30, 60, and 90% lower average emissions for electricity (around 720gCO2-eq/kWh, 410gCO2-eq/kWh, and 100gCO2-eq/kWh, respectively). In addition to South-Africa, vanadium is produced in US, Russia, China and some other countries such as Switzerland, Taiwan, Germany, and Brazil [56].
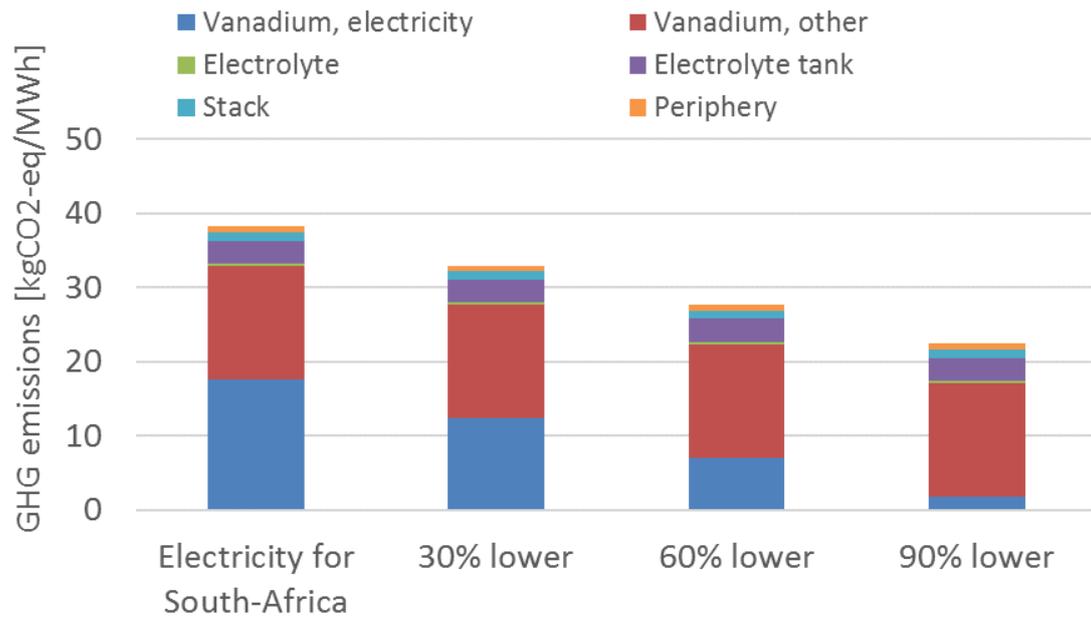
Figure 32: Illustration of the impact of 30, 60, and 90 % lower emissions for electricity production to the total emission. Original result, 38.2kgCO2-eq/MWh is from Weber et al. [53], and the total emission is estimated per MWh of electricity delivered by battery over lifetime (20 years).

7.5   Conclusions and further research needs

In the screening of the LCA of batteries, the authors studied the relevant LCA calculation guidelines, analysed research articles and life cycle inventory databases to find average values for global warming potentials of batteries focusing on NCM-batteries. The best available input data and Ecoinvent database was utilized to create a LCA calculation model for NCM and LFP battery cradle-to-gate phases. Also GWP values for the redox flow battery were searched and analysed from the literature. Technical battery specifications were requests from INVADE pilot representatives.

It was noted, that the data on remanufacturing of LIBs was scarce, even in the literature. It was also found that the different literature studies lead often down to the same base study. For VRFB, only one relevant study was found. Thus, the diversity of battery life cycle inventory data needs to be increased. Many studies use already produced data as the data source, which lead to rather old data age. The reliability of results could be increased the more industry specific data.

The second life batteries were identified as an interesting topic for future research. There are no clear guidelines on how to address shift from the first to the second life cycle. The SOH factor was identified as a suitable factor determining the usability of retired batteries in the second life batteries.

References

[1]   S. Jenu, A. Hentunen, S. Tuurala and A. Manninen, "Simplified state of health diagnostics tool," Deliverable D6.3, EU-INVADE, 2018.

[2]   A. Hentunen, J. Forsström, S. Jenu, V. Mukherjee, S. Tuurala, A. Manninen and S. Bjarghov, "Advanced battery techno-economics tool," Deliverable D6.5, EU-INVADE, 2018.

[3]   P. Gjerløw, "Pilot specifications v3.0," Deliverable D10.1, EU-INVADE, 2018.

[4]   M. Ecker, N. Nieto, S. Käbitz, J. Schmalstieg, H. Blanke, A. Warnecke and D. Sauer, "Calendar and cycle life study of Li(NiMnCo)O2-based 18650 lithium-ion batteries," *Journal of Power Sources,* vol. 248, pp. 839-851, 2014.

[5]   S. Käbitz, J. Gerschler, M. Ecker, Y. Yurdagel, B. Emmermacher, D. André, T. Mitsch and D. Sauer, "Cycle and calendar life study of a graphite|LiNi1/3Mn1/3Co1/3O2 Li-ion high energy system. Part A: Full cell characterization," *Journal of Power Sources,* vol. 239, pp. 572-583, 2013.

[6]   S. Rothgang, M. Rogge, J. Becker and D. U. Sauer, "Battery Design for Successful Electrification in Public Transport," *Energies,* vol. 8, pp. 6715-6737, 2015.

[7]   J. Wang, J. Purewal, P. Liu, J. Hicks-Garner, S. Soukazian, E. Sherman, A. Sorenson, L. Vu, H. Tataria and M. Verbrugge, "Degradation of lithium ion batteries employing graphite negatives and nickel cobalt manganese oxide + spinel manganese oxide positives: Part 1, aging mechanisms and life estimation," *Journal of Power Sources,* vol. 269, pp. 937-948, 2014.

[8]   E. Sarasketa-Zabala, I. Gandiaga, E. Martinez-Laserna, L. Rodriguez-Martinez and I. Villareal, "Cycle ageing analysis of a LiFePO4/graphite cell with dynamic model validations: Towards realistic lifetime predictions," *Journal of Power Sources,* vol. 275, pp. 573-587, 2015.

[9]   N. Omar, M. Monem, Y. Firouz, J. Saminen, J. Smekens, O. Hegazy, H. Gaulons, G. Mulder, P. Van den Bossche, T. Coosemans and J. Van Mierlo, "Lithium iron phosphate based battery – Assessment of the aging parameters and development of cycle life model," *Applied Energy,* vol. 113, pp. 1575-1585, 2014.

[10] Valence Technology, *XP Modules Datasheet,* Lithium Werks, 2017.

[11] J. Peters, M. Baumann, B. Zimmermann, J. Braun and M. Weil, "The environmental impact of Li-Ion batteries and the role of key parameters - A review," *Renewable and Sustainable Energy Reviews,* vol. 67, pp. 491-506, 2017.

[12] B. Xu, A. Oudalov, A. Ulbig, G. Andersson and D. Kirschen, "Modeling of Lithium-Ion Battery Degradation," *IEEE Transactions on Smart Grid,* vol. 9, no. 2, pp. 1131-1140, 2018.

[13] J. Jiang, W. Shi, Zheng, J, P. Zuo, J. Xiao, X. Chen, W. Xu and J.-G. Zhang, "Optimized Operating Range for Large-Format LiFePO4/Graphite Batteries," *Journal of The Electrochemical Society,* vol. 161, no. 3, pp. A336-A341, 2014.

[14] F. Richter, P. Vie, S. Kjelstrup and O. Burheim, "Measurements of ageing and thermal conductivity in a secondary NMC-hard carbon Li-ion battery and the impact on internal temperature profiles," *Electrochimica Acta,* vol. 250, pp. 228-237, 2017.

[15] K. Jalkanen, J. Karppinen, L. Skogström, T. Laurila, M. Nisula and K. Vuorilehto, "Cycle aging of commercial NMC/graphite pouch cells at different temperatures," *Applied Energy,* vol. 154, pp. 160-172, 2015.

[16] L. Tan, L. Zhang, Q. Sun, M. Shen, Q. Qu and H. Zheng, "Capacity loss induced by lithium deposition at graphite anode for LiFePO4/graphite cell cycling at different temperatures," *Electrochimica Acta,* vol. 111, pp. 802-808, 2013.

[17] J. Groot, M. Swierczynski, A. Stan and S. Kær, "On the complex ageing characteristics of high-power LiFePO4/graphite battery cells cycled with high charge and discharge currents," *Journal of Power Sources,* vol. 286, pp. 475-487, 2015.

[18] J. Schmitt, A. Maheshwari, M. Heck, S. Lux and M. Vetter, "Impedance change and capacity fade of lithium nickel manganese cobalt oxide-based batteries during calendar aging," *Journal of Power Sources,* vol. 353, pp. 183-194, 2017.

[19] M. Ecker, J. Gerschler, J. Vogel, S. Käbitz, F. Hust, P. Dechent and D. Sauer, "Development of a lifetime prediction model for lithium-ion batteries based on extended accelerated aging test data," *Journal of Power Sources,* vol. 215, pp. 248-257, 2012.

[20] M. Lewerenz, J. Münnix, J. Schmalstieg, S. Käbitz, M. Knips and D. Sauer, "Systematic aging of commercial LiFePO4jGraphite cylindrical cells including a theory explaining rise of capacity during aging," *Journal of Power Sources,* vol. 345, pp. 254-263, 2017.

[21] S. Grolleau, A. Delaille, H. Gualous, P. Gyan, R. Revel, J. Bernard, E. Redondo-Iglesias and J. Peter, "Calendar aging of commercial graphite/LiFePO4 cell - Predicting capacity fade under time dependent storage conditions," *Journal of Power Sources,* vol. 255, pp. 450-458, 2014.

[22] E. Redonso-Iglesias, P. Venet and S. Pelissier, "Eyring acceleration model for predicting calendar ageing of lithium-ion batteries," *Journal of Energy Storage,* vol. 13, pp. 176-183, 2017.

[23] S. Wu and P.-H. Lee, "Storage fading of a commercial 18650 cell comprised with NMC/LMO cathode and graphite anode," *Journal of Power Sources,* vol. 349, pp. 27-36, 2017.

[24] Samsung SDI, "ESS Batteries by Samsung SDI," [Online]. Available: http://www.samsungsdi.com/upload/ess_brochure/201803_SamsungSDI%20ESS_EN.pdf. [Accessed 20 11 2018].

[25] *Smart Battery Systems for Energy Storage,* Samsung SDI, 2016.

[26] Tesvolt, "Lithium Storage System TS HV 70," [Online]. Available: https://www.tesvolt.com/templates/tesvolt/files/pdf/E.DB.TSHV.ENG-A.26.pdf. [Accessed 20 11 2018].

[27]   M. J. E. Alam and T. K. Saha, "Cycle-Life Degradation Assessment of Battery Energy Storage Systems Caused by Solar PV Variability," *Power and Energy Society General Meeting (PESGM), IEEE,* pp. 1-5, 2016.

[28]   S. Saxena, C. Le, J. Macdonald and Moura, S., "Quantifying EV battery end-of-life through analysis of travel needs with vehicle powertrain models," *Journal of Power Sources,* vol. 282, pp. 265-276, 2015.

[29]   M. O. Ramoni and H. Zhang, "End-of-life (EOL) issues and options for electric vehicle batteries," *Clean Technologies and Environmental Policy,* vol. 15, no. 6, pp. 881-891, 2013.

[30]   United States Advanced Battery Consortium (USABC), *Electric vehicle battery test procedures manual, revision 2,* 1996.

[31]   V. Ruiz, "Standards for the performance assessment of electric vehicle batteries Study - Possible performance criteria for an Ecodesign Regulation," EUR 29371 EN, Publications Office of the European Union, ISBN 978-92-79-94179-5, Luxembourg, 2018.

[32]   EUROBAT E-Mobility, "Battery R&D Roadmap 2030. Battery Technology for Vehicle Applications," 2015.

[33]   E. Martinez-Laserna, I. Gandiaga, E. Sarasketa-Zabala, J. Badeda, D. I. Stroe, M. Swierczynski and A. Goikoetxea, "Battery second life: Hype, hope or reality? A critical review of the state of the art," *Renewable and Sustainable Energy Reviews,* 2018.

[34]   E. Martinez-Laserna, E. Sarasketa-Zabala, D. I. Stroe, M. Swierczynski, A. Warnecke, J. M. Timmermans, S. Goutam and P. Rodriguez, "Evaluation of lithium-ion battery second life performance and degradation," *2016 IEEE Energy Convers. Congr. Expo,* pp. 1-7, 2016.

[35]   E. Martinez-Laserna, E. Sarasketa-Zabala, I. Villarreal Sarria, D. I. Stroe, M. Swierczynski, A. T. J. M. Warnecke, S. Goutam, N. Omar and P. Rodriguez, "Technical Viability of Battery Second Life: A Study from the Ageing Perspective," *IEEE Trans. Ind. Appl.,* vol. 54, no. 3, pp. 2703-2713, 2018.

[36] R. Spotnitz, "Simulation of capacity fade in lithium-ion batteries," *Journal of Power Sources,* vol. 113, no. 1, pp. 72-80, 2003.

[37] S. Bobba, A. Podias, F. Di Persio, M. Messagie, P. Tecchio, M. A. Cusenza, U. Eynard, F. Mathieux and A. Pfrang, "Sustainability Assessment of Second Life Application of Automotive Batteries (SASLAB): JRC Exploratory Research (2016-2017): Final technical report: August 2018," EUR 29321 EN, Publications Office of the European Union, JRC112543, Luxembourg, 2018.

[38] M. Myllysilta, I. Deviatkin, S. Jenu, I. Munne, S. Tuurala, A. Hentunen and T. Pajula, "Life cycle assessment of first and second-life lithium-ion batteries: Implications from existing studies," in *Symposium proceedings, Towards a Resource Efficient Economy*, Vienna, Austria, November 26-29, 2018.

[39] G. Wernet, C. Bauer and B. Steubing, "The ecoinvent database version 3 (part I): overview and methodology," *International Journal of Life Cycle Assessment,* vol. 21, pp. 1218-1230, 2016.

[40] J. Peters and M. Weil, "Providing a common base for life cycle assessments of Li-Ion batteries," *Journal of Cleaner Production,* vol. 171, p. 704–713, 2018.

[41] G. Majeau-Bettez, T. Hawkins and A. Strømman, "Life Cycle Environmental Assessment of Lithium-Ion and Nickel Metal Hydride Batteries for Plug-In Hybrid and Battery Electric Vehicles," *Environmental Science & Technology,* vol. 45, no. 10, p. 4548–4554, 2011.

[42] L.-W. Ellingsen, G. Majeau-Bettez, B. Singh, A. Srivastava, L. Valøen and A. Strømman, "Life Cycle Assessment of a Lithium-Ion Battery Vehicle Pack," *Journal of Industrial Ecology,* vol. 18, no. 1, pp. 113-124, 2014.

[43] H. Ambrose and A. Kendall, "Effects of Battery Chemistry and Performance on the Life Cycle Greenhouse Gas Intensity of Electric Mobility," *Transportation Research Part D: Transport and Environment,* vol. 47, pp. 182-194, 2016.

[44] H. C. Kim, T. J. Wallington, R. Arsenault, C. Bae, S. Ahn and J. Lee, "Cradle-to-Gate Emissions from a Commercial Electric Vehicle Li-Ion Battery: A Comparative

Analysis," *Environmental Science and Technology,* vol. 50, no. 14, pp. 7715-7722, 2016.

[45] United States Environmental Protection Agency, "Application of Life-Cycle Assessment to Nanoscale Technology: Lithium-Ion Batteries for Electric Vehicles," EPA, 2013.

[46] A. Moro and L. Lonza, "Electricity carbon intensity in European Member States: Impacts on GHG emissions of electric vehicles," *Transportation Research Part D: Transport and Environment,* 2017.

[47] "Renewable electricity output (% of total electricity output)," World Bank, 2018. [Online]. Available: http://databank.worldbank.org/data/reports.aspx?source=2&series=EG.ELC.RN EW.ZS. [Accessed 23 10 2018].

[48] X. Zeng, J. Li and N. Singh, "Recycling of spent lithium-ion battery: A critical review," *Critical Reviews in Environmental Science and Technology,* vol. 44, pp. 1129-1165, 2014.

[49] L. Ellingsen, B. Singh and A. H. and Strømman, "The Size and Range Effect: Lifecycle Greenhouse Gas Emissions of Electric Vehicles," *Environmental Research Letters,* vol. 11, no. 5, 2016.

[50] B. Li, X. Gao, J. Li and C. Yuan, "Life Cycle Environmental Impact of High-Capacity Lithium Ion Battery with Silicon Nanowires Anode for Electric Vehicles," *Environmental Science & Technology,* vol. 48, no. 5, pp. 3047-3055, 2014.

[51] K. Richa, C. W. Babbitt, N. G. Nenadic and G. Gaustad, "Environmental Trade-Offs across Cascading Lithium-Ion Battery Life Cycles," *International Journal of Life Cycle Assessment,* vol. 22, no. 1, pp. 66-81, 2017.

[52] L. C. Casals, B. A. García, F. Aguesse and A. Iturrondobeitia, "Second Life of Electric Vehicle Batteries: Relation between Materials Degradation and Environmental Impact," *International Journal of Life Cycle Assessment,* vol. 22, no. 1, pp. 82-93, 2017.

[53] S. Weber, J. Peters, M. Baumann and M. Weil, "Life Cycle Assessment of a Vanadium Redox Flow Battery," *Environ. Sci. Technol.,* vol. 52, p. 10864–10873, 2018.

[54] C. Zhang, L. Zhang, Y. Ding, S. Peng, X. Guo, Y. Zhao, G. He and G. Yu, "Progress and prospects of next-generation redox flow batteries," *Energy Storage Mater.,* vol. 15, p. 324–350, 2018.

[55] "Ecoinvent Database 3.5," Swiss Centre for Life Cycle Inventories, 2018. [Online]. Available: https://www.ecoinvent.org/ .

[56] US National Minerals Information Center , 2018. [Online]. Available: https://minerals.usgs.gov/minerals/pubs/commodity/vanadium/.